J. Hydrol. Hydromech., 74, 2026, 1, 36–56
https://doi.org/10.2478/johh-2026-0004
©2026 Abdorreza Kabiri-Samani, et al., published by Slovak Academy of Sciences.
This work is licensed under the Creative Commons Attribution-NonCommercial-NoDerivatives 4.0 International Licence.

Journal of Hydrology and Hydromechanics

Does an Armor Layer Control Clear-Water Scour at Cylindrical Bridge Piers? A Comprehensive Experimental Assessment under Steady and Unsteady Flow Conditions

Abdorreza Kabiri-Samani[1*], Amirhossein Fathi[1], Rashid Farooq[2,3]

[1] Department of Civil Engineering, Isfahan University of Technology, P.O. Box 84156, Isfahan, Iran.
[2] Department of Civil and Construction Engineering, Swinburne University of Technology, Melbourne, VIC, 3122, Australia.
[3] Department of Civil Engineering, International Islamic University, Islamabad 44000, Pakistan.
[*] Corresponding author. E-mail: akabiri@cc.iut.ac.ir

Abstract: Local scour at bridge piers is a critical phenomenon jeopardizing structural integrity worldwide. This study presents a comprehensive physical modelling investigation into the evolution of local scour in the presence of a protective armor layer, considering both steady and unsteady (hydrograph) flow regimes. A systematic parametric analysis evaluated the effects of pier diameter, flow velocity, and sediment characteristics, the latter comprising three distinct sizes for both the underlying bed material and the armor layer. Experimental observations elucidate the initial scour mechanism: the formation of strong horseshoe vortices that first accumulate armor material upstream of the pier. Subsequent vortex strengthening induces flow instability, leading to the entrainment and downstream transport of bed sediments. Under steady-flow conditions, the maximum equilibrium scour depth shows a strong positive correlation with pier diameter. A 33.3% increase in diameter resulted in a 31.2% increase in scour depth, while a 47.6% increase led to a 46.3% increase. Conversely, the maximum scour depth is inversely proportional to the size of both the armor layer particles and the underlying bed material. For unsteady flows, the peak scour depth was determined to be independent of the sequence of hydrograph events, converging to a value equivalent to the equilibrium scour depth of a steady flow at the hydrograph's peak discharge. However, the temporal evolution of scour depth varied significantly between the flow regimes. A dimensional analysis of the experimental data identified the governing dimensionless parameters. This analysis formed the foundation for deriving new predictive equations to estimate the maximum scour depth at bridge piers protected by an armor layer under both steady and unsteady flow conditions. The proposed relationships provide practical tools for the design and risk assessment of bridge piers.

Keywords: Equilibrium depth; Equilibrium time; Horseshoe vortexes; Hydrograph; Image processing; Maximum scour depth.

1 INTRODUCTION

Under certain circumstances, when proper scour control measures are not employed, the flow around bridge piers results in local scouring, which can lead to the destruction of the piers and, consequently, the failure of the entire bridge structure. Bridge pier scouring is a major cause of bridge failure, often without warning, resulting in human fatalities and economic losses worldwide every year (Wang et al., 2017; Bento et al., 2020; Sammen et al., 2025). Numerous researchers have developed equations and algorithms to estimate the maximum and/or equilibrium scour depth under steady flow conditions, such as Raudkivi and Ettema (1983), Kandasamy and Melville (1998), and Melville and Sutherland, (1988). Furthermore, fundamental mechanistic models, such as the one proposed by Guo (2012), which conceptualize scour in terms of the pressure gradient through flow-structure-sediment interactions, provide a physical basis for scour prediction and design. However, the transient and complex nature of unsteady flow scour, such as during flood hydrographs, introduces additional dynamics that are less captured by these steady-state models and necessitate specific consideration. Considering the significant risk posed by scour, a critical area of research involves developing effective countermeasures. Among the various methods reviewed in the introduction section for reducing scour at bridge piers, the use of armor layer has emerged as a prominent approach for scour reduction. This study, therefore, establishes a consolidated understanding of the scour process, encompassing both steady and unsteady flow regimes, before proceeding to a detailed evaluation of armor layers as a specific and widely used mitigation technique.

Gaudio et al. (2012) presented the results of clear-water scouring tests on five combined flow-altering countermeasures against bridge pier scours. The results clarify that an improper combination of two countermeasures may be less effective than each countermeasure. Link et al. (2018) investigated the feasibility of physical modeling techniques for the quantification of prototype bridge pier scours in reduced-scale models. They declared that the scour process at a bridge pier is controlled by the dimensionless effective flow work and the dimensionless grain diameter. Valela et al. (2018) investigated the reduction of bridge pier scour using a novel collar design, declaring that their proposed design reduces scour depth. Tipireddy and Barkdoll (2019) experimentally investigated the reduction of scour by injecting air into the cylindrical bridge piers. They found that air injections reduce the scour around the piers to a negligible level. Delf Lovimi et al. (2020) studied the effectiveness of the combined use of cables and collars to control scouring at bridge piers. Ranjbar-Zahedani et al. (2021) proposed a submerged triangular flow diversion structure to reduce local scour around bridge piers. Different dimensions, locations, and submergence ratios were examined based on model experimentation. They found that the optimized structure resulted in a 40% reduction in the maximum scour depth and a 60% reduction in the scour volume. Valela et al. (2021) investigated hybrid modeling for the design of new bridge piers, collars, and improved bridge pier collars to reduce scour, reporting that the combination of the new abutment collar design with other ancillary structures significantly reduces scour. Okhravi et al. (2022) conducted an experimental study on local scouring at single pile and 1×4 piles group in uniform and non-uniform bed sediments under clear water conditions, suggesting that the effects of sediment grading decreased by increasing flow depth. Furthermore, they stated that the maximum scouring depth in piles group generally increased by decreasing the pile spacing for uniform sediments. The aforementioned trend was not observed for non-uniform sediments for the same hydraulic conditions. Their experimental results also showed that bed sediment grading is a controlling factor in pile scouring. Abdi-Chooplou et al. (2023) conducted experiments on the effects of submerged plates with full overlap length across the channel on local scouring at a 180-degree bridge pier, showing that submerged plates reduce the scour depth around bridge piers. Through laboratory experiments, Farooq et al. (2023) demonstrated that a hook collar significantly reduces scour around a lenticular pier. Their key findings include i) equilibrium scour depth decreases with the collar-to-pier width ratio, ii) scour depth decreases as the collar wall height increases to 0.3 the pier width, and iii) placement on the bed surface provides the maximum efficiency. Ahmadi et al. (2025) investigated the effectiveness of a new scour control measure, namely porous basket, modifying the flow structure and reducing scour around elliptical and hexagonal piers. Their results showed that piers with aspect ratio equal to 5 experienced a 50% reduction in scour volume, because of reducing Reynolds' Shear Stress in the downflow region. Researchers such as Moncada et al. (2009), Pandey et al. (2023), Farooq et al. (2021), Gupta et al. (2023), Dehghan et al. (2023), Baranwal and Das (2024), and Vaghefi et al. (2025) have also conducted extensive studies on the scour at bridge piers under steady flow conditions.

Some researchers have attempted to derive relationships to relate the maximum scour depth to the hydraulic characteristics of steady flow conditions. Notably, steady-state flow is not realistic in most river engineering problems, in which unsteady flow is typically established, causing destructive floods in a short period of time. Therefore, designing river structures based on steady-state flow is unreasonable and is occasionally not economical (Hager and Unger, 2010, and Karimaei and Zarrati, 2019a). Therefore, scouring under unsteady flow conditions has been the focus of several other researchers (Chang et al., 2004). Kothyari et al. (1992) simulated unsteady flow conditions as a series of step-type steady-state flow hydrographs with a duration of 5 minutes. Compared to their experimental data, they concluded that the proposed method precisely predicts the scour hole geometry. They reported that the shape of triangular hydrographs does not significantly affect the scour depth. Borghei et al. (2012) conducted an extensive experimental study on how different unsteady flow hydrograph shapes affect scour at bridge piers found on a uniform sediment bed. Based on the work of Kothyari et al. (1992), Bento et al. (2018) experimentally investigated bridge pier scouring under unsteady flow conditions and compared their findings with those of the predecessor study. Karimaei and Zarrati (2019b) investigated the temporal local scour depth at a rectangular bridge pier under unsteady flow conditions and suggested that the shorter the rising limb of the hydrograph (or the sharper the hydrograph), the greater the rate of sediment transport towards the downstream. Eshaghian et al. (2020) investigated scouring at bridge piers with uniform and non-uniform sediments. They declared that by increasing the flow discharge, the maximum scour depth increases, and a coarser armor layer is formed around the pier inside the scour hole. Misuriya and Eldho (2023) investigated the effect of turbulent structures on the local scouring of a cylindrical pier under unsteady flow conditions. They limited their study to triangular-shaped flood hydrographs, stating that hydrograph shapes can vary in real-world scenarios. Solati et al. (2023) investigated the scour pattern around a pier in a sharp 180° bend, considering different base shapes of unsteady flow hydrographs. Their results showed that the maximum scour depth downstream of piers with different shapes is a function of the duration of the unsteady flow. Solati et al. (2024) investigated scour and bed morphology dynamics in a sharp bend with a collar under unsteady flow conditions. Their results showed that the collar successfully reduces the maximum scoured hole depth, volume, and area around the pier by more than 95 percent.

The use of a riprap, armor layer, and layered soils is a common technique to mitigate scour by enhancing the bed's resistance. A foundational study by Lim and Chiew (2001) systematically investigated the parameters influencing riprap stability around a cylindrical bridge pier in uniform bed materials. Their results indicated that within the upper dune regime, variations in these parameters did not affect the mechanism of embedment failure. The armor layer increases the critical shear velocity for bed particles, reaching the threshold of the movement stage (Dey and Barbhuiya, 2004, and Babakhah and Khoshfetrat, 2024). As the scour hole deepens, a secondary armor layer with a thickness equal to the particle diameter develops inside the hole, which prevents further scouring. The reinforcement provided by a secondary armor layer stabilizes the scour hole surface, thereby reducing the ultimate scour depth (Van Rijn, 1984). Several theories have been developed to explain the mechanisms through which the armor layer influences scour. For instance, Raudkivi and Ettema (1984) proposed that an armor layer will not form for sediments with a geometric standard deviation (σ_g) of less than 1.5. Furthermore, Dey and Barbhuiya (2004) emphasized that for non-uniform sediments, particle size significantly governs the scour depth. They specifically concluded that the observed reduction in scour depth is attributable to the formation of an armor layer within the scour hole. Dey and Raikar (2007) conducted experiments on circular piers with a sandy bed and a sandy armor layer, indicating that the equilibrium scour depth is meaningfully less than that without an armor layer, provided that a secondary armor layer is formed in the scour hole. Muzzammil and Siddiqui (2009) developed a methodology for the reliability assessment of bridge pier scour in non-uniform sediments using the first-order reliability method (FORM). Their study included a sensitivity analysis to evaluate the influence of various random variables on pier reliability against scouring. In a complementary approach, Raikar and Dey (2009) synthesized prior experimental results to derive an equation for estimating the final scour depth that explicitly accounts for the armor layer of particle size. Sui et al. (2010) and Maherani et al. (2010) investigated the effects of the armor layer on scouring under steady flow conditions for semicircular and semielliptical abutments. They declared that the scour depth increases by increasing the bed particle size in the presence of a constant particle size armor layer. Pandy et al. (2019) investigated scour at a cylindrical bridge pier under the presence of an armor layer in a steady flow condition, indicating that the maximum scour depth is not only a function of the flow parameters but also depends on the size and geometric standard deviation of the bed and armor layer materials. Karkheiran et al. (2021) applied the experimental data, documented in a pioneer work by Kabiri-Samani (2012a and b), to investigate scour at bridge piers in uniform and armored beds, under steady and unsteady flow conditions, applying feed-forward back-propagation artificial neural network (FFBP-ANN) combined with evolutionary algorithms, including adaptive particle swarm optimization (APSO) and genetic algorithms (GA). Accordingly, they reported that the ANN-APSO model is the best tool to evaluate the scour depth at bridge piers in uniform sediment beds. Whereas the ANN-GA algorithm has the best fitness values in uniform and armored sediment beds under unsteady flow conditions. Valela et al. (2022) declared that creating a new design around the bridge pier and installing a gap layer around the pier flush with the surrounding bed significantly reduces the strength of the horseshoe vortex. They also stated that riprap is beneficial in preserving infrastructure and increasing public safety around the piers. Investigations into multi-layer sediments have provided critical insights. For instance, Wang et al. (2022) studied scour around piles in single- and double-layer sediments of varying grain sizes. Their key finding was a distinct division of influence: the properties of the overlying soil layer controlled the onset of erosion and the ultimate lateral extent of the scour hole, and the properties of the underlying layer determined the final scour depth. Based on their experimental results, they subsequently proposed an innovative predictive framework for scour depth in two-layer sediment systems. Further supporting the influence of sediment stratification, Veldhuizen et al. (2023) also investigated scour development in layered soils around offshore monopile foundations. Their research demonstrated that a top layer of sand, when compared to vertically homogeneous soils, can lead to two significant effects: a substantial reduction in the maximum scour depth and an increase in the non-uniformity of the scour hole geometry. As another physical modeling study, Zefzouf et al. (2025), investigated monopile scour in layered, non-cohesive soils under steady clear-water flow. They reported that a higher uniformity coefficient led to scour depths similar to single-layer coarse sand, and identified top-layer scour as an effective predictor of the scour rate. Their findings were formulated into design implications for dynamic scour protection.

The use of artificial armor layers is a well-established technique for controlling scouring at bridge piers. However, current design methods often lack comprehensive guidance for conditions beyond steady-state flow, and there is a need for more robust correlations that can predict scour depth accurately under the dynamic, unsteady flow conditions typical of real-world floods. Building upon our foundational investigations (Kabiri-Samani 2012a, b), this study presents a significant experimental advancement in quantifying clear-water scour at bridge piers protected by an armor layer. Considering the critical role of armor in protecting erodible beds, we conducted a comprehensive parametric study to address the limitations of existing design methods, which often rely on steady-state assumptions. This study experimentally investigates how scour development is governed by the interplay between hydraulic conditions (flow velocity), structural geometry (pier diameter), and soil properties (both the unprotected bed and the armor layer). A key innovation was the use of an image processing technique to capture high-resolution, three-dimensional scour topography, providing a superior dataset for analysis. Crucially, to bridge the gap between laboratory conditions and real-world scenarios, we extended the study beyond steady flow to include unsteady flow conditions, simulated through a series of hydrographs with varying base times and repetition numbers. Through dimensional analysis of this extensive dataset, we have developed refined correlations for predicting equilibrium scour depth. These improved models offer the following practical benefits:

For steady-flow design, it provides a more reliable means of measuring armor layers under peak flood discharge (a common design standard) for a wide range of pier, bed, and armor characteristics. For unsteady flow risk assessment, this is the primary contribution. Our relationships explicitly model the cumulative effect of flood hydrographs, allowing engineers to assess scour damage not just from a single peak event, but from repeated flood cycles or a complex going giving and down limb. Move beyond conservative, and potentially costly designs based solely on the maximum steady velocity, towards more efficient and resilient designs that consider the actual hydraulic history a pier will endure. Nevertheless, this work provides practitioners with enhanced, experimentally validated tools for the design and risk assessment of bridge pier scour protection, explicitly accounting for the dynamic nature of real river flows, thereby contributing to more resilient hydraulic infrastructure.

2 VARIABLES AND DIMENSIONAL ANALYSIS

Figure 1 shows the parameters affecting the maximum scour depth at a bridge pier in the presence of an armor layer, and Eq. (1) lists the parameters affecting the maximum scour depth at a circular bridge pier with an armor layer under unsteady flow conditions.

$$d_{s,u} = f(V_e, y, B, d_{50}, d_a, S, T, t, t_e, n, g, \mu, \rho_w, \rho_s) \tag{1}$$

where $d_{s,u}$ is the maximum scour depth under unsteady flow conditions, $V_e = U - 0.5U_{ca}$ the critical bed velocity (Sui et al. 2010), U_{ca} the average critical flow velocity of the armor layer particles, U the average flow velocity, y the flow depth, B the pier diameter, d_{50} the median bed particle size, d_a the median armor layer size, S the armor layer thickness, T the base time of the unsteady flow hydrograph, t the time, t_e the scouring equilibrium time, n the number of repetition of the hydrograph, g the gravitational acceleration, μ the fluid dynamic viscosity, ρ_w the fluid density, and ρ_s the sediment material density. In the present study, the flow depth was kept constant at y = 0.07 m (Karimaei and Zarrati, 2019a and Abdi-Chooplou et al., 2023). Furthermore, the thickness of the armor layer was approximately three times the median particle size of the armor layer $3d_a$ (Raudkivi and Ettema 1984; Dey and Barbhuiya 2004; Dey and Raikar 2007; Raikar and Dey 2009). Accordingly, the parameters y and S were removed from further analysis, and therefore, Eq. (1) yields Eq. (2):

$$d_{s,u} = f(V_e, B, d_{50}, d_a, T, t, t_e, n, g, \mu, \rho_w, \rho_s) \tag{2}$$

Considering V_e, ρ_w, and B as the repetitive parameters and applying the Buckingham π theorem, the maximum scour depth at bridge piers under unsteady flow conditions is related to the following dimensionless parameters:

$$\frac{d_{s,u}}{B} = f(\frac{d_{50}}{B}, \frac{d_a}{B}, \frac{TV_e}{B}, \frac{t}{t_e}, n, F, R) \tag{3}$$

Where F = $V_e/(\Delta gB)^{0.5}$, R = $\rho_w V_e B/\mu$ are the bridge pier Froude and Reynolds numbers (Valela et al., 2018), $\Delta g = g(G_s\text{-}1) = g[(\rho_s\text{-}\rho_w)/\rho_w]$ is the reduced gravitational acceleration due to buoyancy, G_s is the specific density. The parameter t/t_e is the time development of the scour hole under steady flow conditions.

Combining the parameters d_{50}/B and d_a/B, the parameter d_a/d_{50} is obtained, defined as the ratio of the armor layer median particle size to the bed median particle size. For a fully developed turbulent flow (R > 2500, which was fully justified in the present experiments) over a coarse bed, the viscosity scale effect is minimal; therefore, the pier Reynolds number (R) is also ignored (Dey and Barbhuiya 2004; Sui et al. 2010). Therefore, the dimensionless equation of the maximum scour depth at a bridge pier under unsteady flow conditions is simplified as:

$$\frac{d_{s,u}}{B} = f\left(\frac{d_a}{d_{50}}, \frac{TV_e}{B}, n, F\right) \quad (4)$$

For a steady-state flow condition, the relative maximum scour depth at the bridge pier in the presence of an armor layer $d_{s,s}/B$ is related to the following dominant dimensionless parameters:

$$\frac{d_{s,s}}{B} = f\left(\frac{d_a}{d_{50}}, \frac{t}{t_e}, F\right) \quad (5)$$

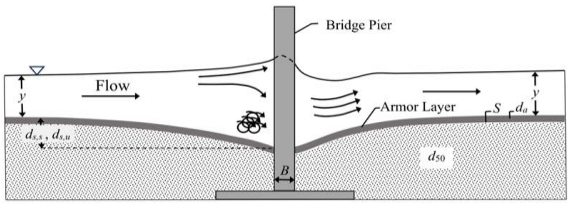

Fig. 1. The parameters affecting the scour at a bridge pier in the presence of an armor layer.

3 MATERIALS AND METHODS

In the present study, experiments were conducted in a horizontal glass-wall water flume 8.5 m long, 0.405 m wide, and 0.7 m deep. The channel sidewalls are made of tempered glass, and the bottom walls are made of galvanized steel sheets. Figure 2 shows a schematic view of the flume and experimental setup, which included gabion mattresses and layers of perforated steel walls to minimize the water level disturbances occurring at the entrance of the flume. According to Raudkivi and Ettema (1983) and Raikar and Dey (2009), the maximum scour depth at bridge piers, located in armored beds, is 3.1B; therefore, considering the maximum pier diameter of 0.042 m, the bed material thickness should be at least 0.13 m. Accordingly, the height of the erodible bed materials was selected as 0.2 m (sufficiently greater than 0.13 m), so that under any circumstances, the scour hole did not reach the bottom of the channel. Piers were installed in the mid-length of a test section 2 m long and 0.2 m high filled with bed sediment, and then the armor layer materials between the two up- and downstream 0.2 m high platforms 5 and 1.5 m long, respectively (Fig. 2). Flow through the closed circuit was supplied using a centrifuge pump with a maximum flow discharge of 0.07 m^3s^{-1}, adjusted by an electromagnetic flow meter with a precision of ±0.2% of the full scale, applying a 0.2 m diameter inlet pipe and two 0.16 m diameter outlet pipes. This type of flow meter measures the instantaneous flow discharge as the average instantaneous flow discharge of millions of points inside the cylinder. Passing through the upstream reservoir and the dissipater walls, the flow was checked to be fully turbulent. For more certainty, the upstream platform was covered by coarse-grained materials, preventing any local inflow-imposed scouring due to the change in bed roughness. Furthermore, velocity profiles were measured at three points: 1.5, 3, and 4.5 m from the beginning of the upstream platform, suggesting close similarity of the velocity profiles and showing logarithmic trends. These findings confirm the development of flow through the test section. The water flow depth was kept constant at 0.07 m. To prevent scouring, before the establishment of favorable test conditions, the armor layer was covered with a metal plate, and then the metal plate was gently removed (similar to Abdi-Chooplou et al. 2024).

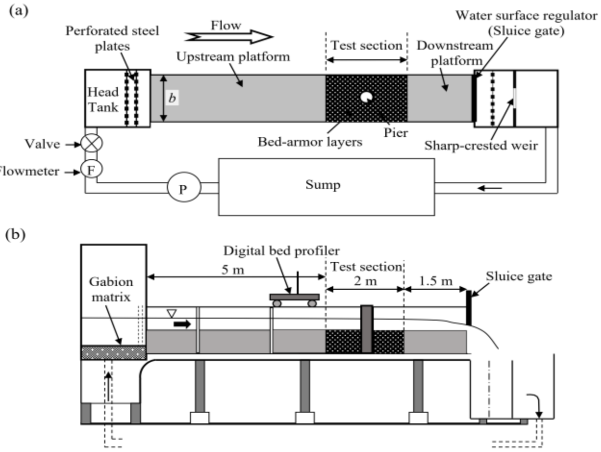

Fig. 2. Schematic of the experimental setup (a) plan view and (b) longitudinal section.

To reduce the effects of the sidewalls, the ratio of the distance between the sidewall and the center of the pier to the diameter of the pier should be greater than 5 (Melville and Chiew, 1999). In the present study, the channel width was 0.405 m, and the maximum pier diameter was limited to 0.042 m. Accordingly, three cylindrical steel piers 0.042, 0.033, and 0.022 m in diameter were employed. To investigate the effect of bed grading on pier scouring, three bed particles with average sizes of 0.00026, 0.00054, and 0.00085 m and three armor layer particles with average sizes of 0.00118, 0.00236, and 0.00356 m were used in the present study (Fig. 3). According to Table 1, the materials used in the bed and the armor layer had a standard deviation $\sigma_g = (d_{84}/d_{16})^{0.5} < 1.6$, categorizing them as uniform grading materials (Zhou et al., 2020 and Parker, 2008). The bed sediment and armor layer materials have a density of 2650 kg m^{-3}. As stated previously, the thickness of the armor layer is mostly 3 times the average particle size of the armor layer. Therefore, in the present study, three armor layer thicknesses of 0.00354, 0.00708, and 0.01068 m were considered. Notably, due to the mixing of the bed and armor layer materials, the test section should be dried at the end of each test.

Table 1. Specifications of the bed and armor layer materials.

Type	d_{50} or d_a (m)	$\sigma_g = (d_{84}/d_{16})^{0.5}$	u^* (m s^{-1})
Bed layer	0.00026	1.25	0.013
	0.00054	1.13	0.016
	0.00085	1.26	0.022
Armor layer	0.00118	1.35	0.026
	0.00236	1.26	0.040
	0.00356	1.26	0.052

The flow equivalent velocity V_e was obtained as $V_e = U - 0.5U_{ca}$ (see Table 2, where U_{ca} is the average critical flow velocity and U the average flow velocity). The average critical flow velocity U_{ca} was determined based on the logarithmic velocity law as $U_{ca}/u^*_{ca} = 5.75 \log[y/(2d_a)] + 6$ (u^*_{ca} is the critical shear velocity of the armor layer particles, Raudkivi and Ettema, 1984). The improved Shields diagram was used to calculate the critical shear velocity u^* (Sui et al., 2010, and Guo, 2020).

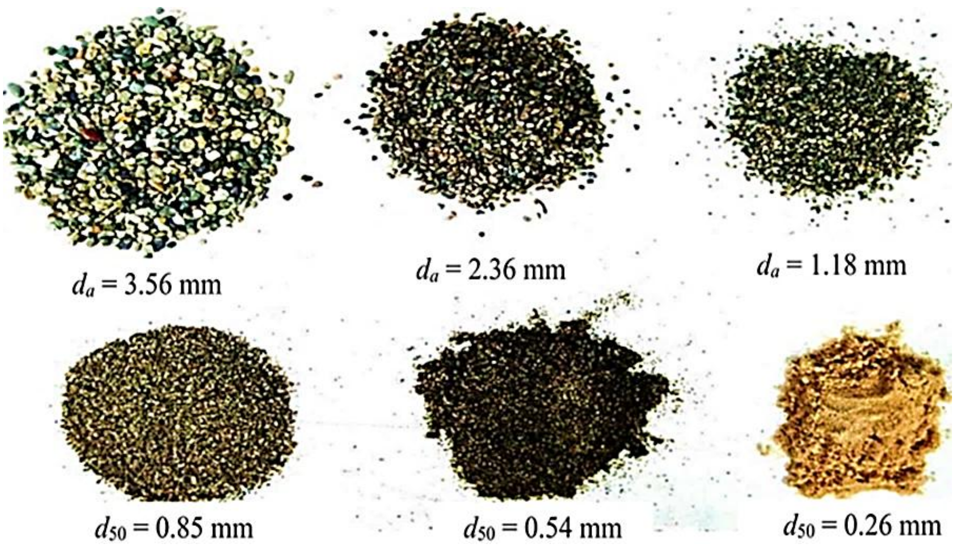

Fig. 3. Bed and armor layers materials, used in the present experiments.

Table 2. The values of V_e for different pier arrangements and for different armor and bed layer materials.

B (m)	d_a/d_{50} (-)	S (m)	$y/(2d_a)$ (-)	u^*_{ca} (m s^{-1})	U_{ca} (m s^{-1})	U (m s^{-1})	V_e (m s^{-1})
0.022, 0.033, 0.042	4.54	0.00354	29.66	0.026	0.376	0.301	0.113
0.022, 0.033, 0.042	9.08	0.00708	14.83	0.040	0.509	0.408	0.154
0.022, 0.033, 0.042	13.69	0.01068	09.83	0.052	0.609	0.487	0.183
0.022, 0.033, 0.042	4.37	0.00708	14.83	0.040	0.509	0.408	0.154
0.022, 0.033, 0.042	6.59	0.01068	09.83	0.052	0.609	0.487	0.183
0.022, 0.033, 0.042	4.19	0.01068	09.83	0.052	0.609	0.487	0.183

3.1 Equilibrium Time, Image Processing, and Bed Topography

According to Chiew (1992), under steady-state flow conditions, the equilibrium scouring time is between 15 and 24 hours. Therefore, based on a trial-and-error procedure, in the present study, we noted that 18 hours satisfactorily achieved the equilibrium scouring depth (Maherani et al., 2010). Establishing the equilibrium scouring depth, the pump was turned off, and the water was gently drained from the scoured hole by a drainpipe. Further to employing a movable bed profiler mounted on the channel sidewalls, moving along and across the flume, to speed up data retrieval, an image processing technique was also applied to determine the final scoured hole geometrical pattern. In the present study, deionized water was slowly added to the scour hole while the drain valve was closed to re-establish the standing water level. Consequently, photos were captured from the scoured hole filled with deionized water by a Nikon D7100 high-speed digital camera with a maximum effective pixel of 24.1 megapixels, a shutter speed range of 30 s to 1/8000 s, and a frame rate of 80 frames/s. Images were processed by an image processing technique using MATLAB software to determine the relationship between the color intensity and the depth of the deionized water at each point. Figure 4a shows an image captured from an experiment. Since working with RGB images is difficult and time-consuming, the color images (Fig. 4a) were converted to grayscale images (Fig. 4b). The color and lights were removed to generate the basic grayscale images for processing (Fig. 4b). Figure 4c shows the contour map of the eroded surface area obtained by the image processing technique. Through image processing, shadows and the lights from the flash of the camera were filtered. To obtain a clear image and reduce noise, a matching noise filter was employed. By converting the color image to a grayscale image and applying mandatory image modifications, the grayscale image was obtained. Consequently, an equivalent matrix was assigned to the image with values corresponding to each pixel of the image, changing between 0 and 255 (0 for black and 255 for white pixels).

Concerning the equivalent matrix of color intensity, in the present study, the deionized water depth was measured at certain points (at least 5 points), which were distributed randomly at different parts of the scoured area, using the digital bed profiler, moving along and across the channel. Then, a graphical relationship was fitted, relating grayscale color intensity and water depth as $h = 30.52e^{-0.035i}$, with a correlation coefficient of 99.6% (where i is the color intensity and h is the deionized water depth). By shrinking the obtained matrix, the coordinates of each pixel were determined and entered into the Surfer software, resulting in sketches that illustrate the topography of the scoured area (Fig. 4c). For more certainty, the results were compared to the directly measured scour depths using the digital bed profiler. The maximum and average uncertainties were 4% and 0.8%, respectively, and more than 95% of the data obtained by the image processing technique were within ±5% of the measured data. Furthermore, as a tool for data analysis, ANOVA (analysis of variance) was used to determine the relative importance of different sources of variation in the datasets. In the present study, statistical analysis of variance was performed using SPSS 19.0 software with one-way ANOVA (SPSS Inc., Chicago, IL, USA). Under unsteady-state flow conditions, the effects of the unsteady hydrograph base time, shape, and number of repetitions were investigated.

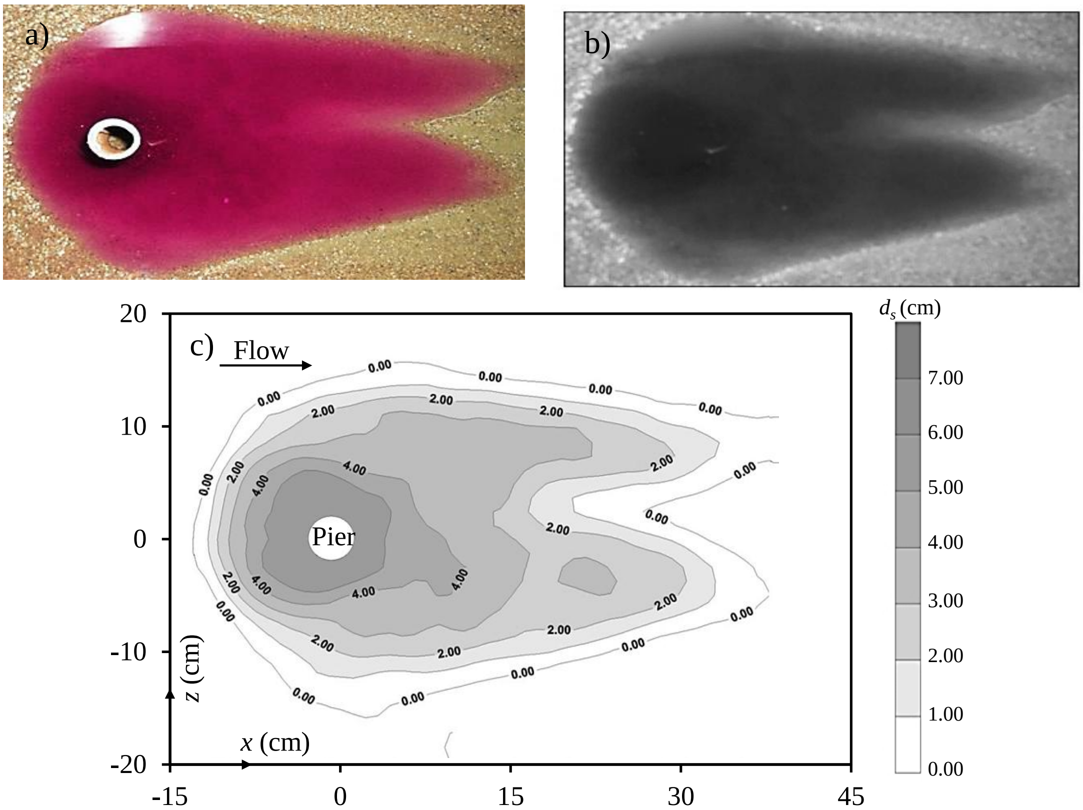

Fig. 4. Image processing to obtain the maximum scour depth: (a) experimental color image, (b) experimental grayscale image, and (c) two-dimensional topography of the scoured area.

3.2 Trend Analysis of Flow Rate Changes

In the present study, ten triangular hydrographs were considered to simulate unsteady flow conditions (Fig. 5). Misuriya and Eldho (2023) and Karkheiran et al. (2021) used the same hydrograph shapes in their studies. As illustrated, an elementary base time of T = 30 min was applied to create 10 hydrograph arrangements, H_1 to H_{10}. Considering three different armor layer average particle sizes of 0.00118, 0.00236, and 0.00356 m, the maximum flow discharges for the considered hydrographs were 0.0085, 0.0114, and 0.0137 m^3s^{-1}, respectively, and the minimum flow discharge was 0.003 m^3s^{-1}, which corresponds to the critical velocity required to initiate the motion of the finest sediment particles within the armor layer, thereby activating the scouring process. To determine the discharge required to the sediment threshold of motion, a constant flow depth was assumed. The critical velocity was then derived by applying the logarithmic law, with the critical shear stress obtained from the improved Shields diagram. Separately, the operational discharge was calculated using the same constant depth and the measured average flow velocities from Table 2.

A backwater effect created a reservoir upstream of the piers (Chaudhry, 2008). Since reservoir flow differs from river flow, a simpler analysis using the continuity equation is appropriate (Hager and Sinniger, 1985; Chow, 1959). Equation (6) models the relationship between the reservoir's inflow (I), outflow (O), and storage volume (S_v) over time (t).

$$I - 0 = \frac{dS_v}{dt} \tag{6}$$

Formerly, to determine the unstable flow rate passing through and at the end of the reservoir, two approaches have been used. The first approach uses the storage equation as a basis (Fiorentini and Orlandini, 2013), and the second approach employs the watershed discharge method for calibration. Through the first approach, the modified pulse method is used (Ghasemzadeh et al., 2020). Ultimately, the outflow rate O is determined using Eq. (7). In Eq. (7), indices 1 and 2 refer to the beginning and end of the considered time step, respectively. First, the relationship between O and $[(2S_v/t + O)]$ is obtained and accordingly, the key routing variable, $[(2S_v/t + O)]$, is determined at each time step via the discrete storage equation (Ghasemzadeh et al., 2020; Hashemi et al., 2025).

$$(I_1 + I_2) + \left(\frac{2S_{v1}}{t} - O_1\right) = \frac{2S_{v2}}{t} + O_2 \tag{7}$$

De Laine (1964) calibrated six major end weirs using the pondage discharge method (Eq. 8, y is the flow depth inside the pond, the subscript h indicates the corresponding parameter value at a specified depth, A_s the surface area of the pond, and dy/dt represents the intensity of flow instability) and reported errors of about 4% for low flows and up to approximately 11% for flows as large as 0.845 m^3 s^{-1}. He stated that a significant portion of the total error could be attributed to errors in recording dy/dt.

$$(I - O)_h = (A_s)_h \left(\frac{dy}{dt}\right)_h \tag{8}$$

Ghasemzadeh et al. (2020) found that the storage equation and modified Puls method showed significant error only at hydrograph breakpoints, with minimal error on the ascending and descending branches. In this study, flow changes were modeled using triangular hydrographs, treating the water behind the weir as a reservoir. Despite the flow supply being at the flume's start, the negligible error in Fig. 5 led to the assumption that inflow and outflow values were equal (Mahdavi et al., 2024). The hydrographs were physically generated and controlled by a programmable logic controller (PLC), ensuring accurate, repeatable simulation of flood waves in both the up- and downstream branches. This method enabled a systematic analysis of the reservoir's response to standard inflow conditions.

Overall, 18 tests were performed under steady-state flow conditions, and 180 tests were conducted under unsteady-state flow conditions. To prevent scale effects resulting from fluid viscosity and surface tension, the water depth should be at least 0.03 m (Sui et al., 2010; Valela et al., 2022). According to the existing criteria in the literature, while Reynolds number R = $\rho_w V_e B/\mu \geq 2500$ (Kabiri-Samani and Naderi, 2017) and Weber number W = $\rho_w B V_e^2/\sigma \geq 100$ (Hsiao et al., 1988), the effects of viscosity and surface tension, respectively, are minimal and negligible. In the present study, for a minimum flow discharge of Q = 0.003 m^3 s^{-1} and a water flow depth of 0.07 m, the minimum Reynolds and Weber numbers were mostly greater than 10000 and 350, respectively. Therefore, the effects of viscosity and surface tension were neglected. Table 3 tabulates the tests performed under unsteady-state flow conditions as well as the maximum scour depths at the bridge pier under unsteady flow conditions.

4 OBSERVATIONS, RESULTS, AND DISCUSSION

4.1 Laboratory Observations

While the flow shear velocity is approximately equal to 50% of the shear velocity of the armor layer particles, scouring around the bridge pier begins. Scouring starts at the sides of the pier and then spreads down- and upstream, expanding over time. Simultaneously, through the development of the scour hole, the armor particles fall down from the upper edge of the scour hole into the hole, forming a secondary armor layer, preventing further scouring. Our observations show that at the start of all experiments, due to continuous feeding of the scour hole by armor material in its upper part, a relatively thick secondary armor layer forms downstream of the pier. However, due to the horseshoe vortex's high strength, this layer is unstable, and the materials are continuously transferred downstream. By increasing the depth of the hole and decreasing the strength of the horseshoe vortex, this layer becomes stable, and the equilibrium scour depth is attained. It should be noted that horseshoe eddies are a critical component in the process of pier scour (Kisi et al., 2023).

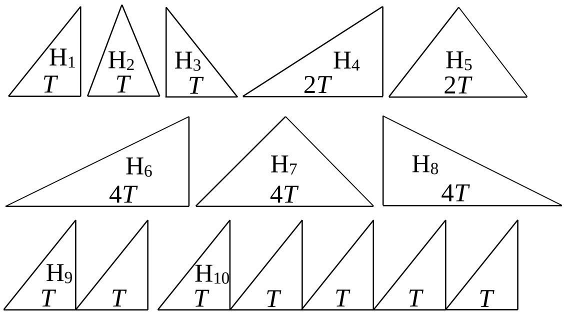

Fig. 5. Types of hydrographs used in the present study for unsteady flow conditions.

Table 3. Maximum scour depth at the pier under unsteady-state flow conditions.

Test specifications				Hydrograph number									
Model	B (m)	d_a/d_{50}	F	H_1	H_2	H_3	H_4	H_5	H_6	H_7	H_8	H_9	H_{10}
-	-	-	-	$d_{s,u}$ (m)									
M_1	0.042	13.69	0.222	0.047	0.048	0.050	0.052	0.050	0.051	0.054	0.052	0.051	0.053
M_2	0.033	13.69	0.250	0.033	0.032	0.035	0.035	0.038	0.036	0.040	0.039	0.036	0.038
M_3	0.022	13.69	0.307	0.008	0.010	0.011	0.009	0.012	0.008	0.011	0.010	0.012	0.011
M_4	0.042	9.08	0.187	0.053	0.055	0.054	0.057	0.058	0.061	0.062	0.060	0.058	0.061
M_5	0.033	9.08	0.211	0.046	0.044	0.047	0.050	0.048	0.052	0.050	0.048	0.049	0.052
M_6	0.022	9.08	0.258	0.024	0.023	0.024	0.026	0.027	0.029	0.029	0.027	0.026	0.029
M_7	0.042	4.54	0.137	0.055	0.054	0.054	0.057	0.058	0.062	0.062	0.061	0.059	0.062
M_8	0.033	4.54	0.155	0.046	0.045	0.047	0.049	0.049	0.054	0.053	0.051	0.050	0.053
M_9	0.022	4.54	0.189	0.030	0.031	0.033	0.034	0.035	0.038	0.038	0.037	0.034	0.037
M_{10}	0.042	6.59	0.222	0.049	0.048	0.051	0.053	0.052	0.055	0.057	0.053	0.053	0.055
M_{11}	0.033	6.59	0.250	0.033	0.034	0.037	0.036	0.037	0.038	0.036	0.037	0.035	0.037
M_{12}	0.022	6.59	0.307	0.025	0.026	0.029	0.030	0.030	0.027	0.026	0.029	0.030	0.031
M_{13}	0.042	4.37	0.187	0.056	0.055	0.055	0.058	0.057	0.062	0.060	0.062	0.057	0.062
M_{14}	0.033	4.37	0.211	0.044	0.044	0.043	0.047	0.048	0.050	0.051	0.049	0.049	0.050
M_{15}	0.022	4.37	0.258	0.024	0.023	0.024	0.025	0.024	0.025	0.027	0.024	0.025	0.027
M_{16}	0.042	4.19	0.222	0.050	0.051	0.051	0.053	0.052	0.054	0.052	0.054	0.052	0.052
M_{17}	0.033	4.19	0.250	0.039	0.037	0.038	0.038	0.039	0.040	0.040	0.041	0.040	0.041
M_{18}	0.022	4.19	0.307	0.026	0.024	0.025	0.025	0.026	0.027	0.030	0.026	0.027	0.029

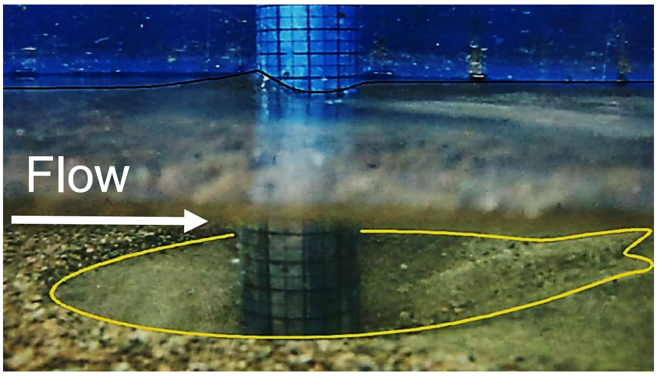

Fig. 6. Scoured hole around a 0.042 m in diameter bridge pier in the presence of the armor layer.

Figure 6 shows local scouring around a 0.042 m in diameter bridge pier in the presence of an armor layer. Observations indicated that the minimum thickness of the stable secondary armor layer is equal to the diameter of the armor layer particles. These particles are arranged in such a way that the least amount of pore space is established, preventing further escape of the underlying materials. However, the armor layer particles are heavier and cannot be easily transported by the existing eddies. At lower flow velocities, fewer particles are transported downstream, and the scour rate is decreased. The armor layer reduces the strength of the jets around the pier and prevents further scouring. Consistent with the conjectural theory of sediment transport and erosion proposed by Einstein (1950), the moving armor particles slowly settle on the bed, and their accumulation increases their mass, impairing the flow's ability to allocate them further. From a practical point of view, excessive shear stress can lead to significant scour depths; therefore, flow can easily move smaller particles downstream. Forming the scoured hole, the secondary armor layer forms inside the scoured bed, reducing the strength of the shear stresses on the bed, preventing further scouring. With an increase in the bed particle size, the flow shear stress has less effect on scouring, thereby cannot easily move larger grains. The scouring process stops when the shear stresses applied to the bed decrease to a critical value (Fathi et al., 2025a, and Dah-Mardeh et al., 2023). Over time, a protective coating of armor layer develops over the bed, decreasing the force exerted on the bed, thereby preventing further erosion. The armor layer reduces the effect of flow shear stress and provides resistance against the movement of larger grains. Also, the scouring phenomenon continues until the shear stress applied to the bed becomes less than or equal to the critical value.

For an armor layer with a 0.00118 m particle size, despite the formation of a secondary armor layer inside the scour hole, this layer had little stability, and even in some cases, due to fluctuations in the downward jet flow, downstream of the pier, the armor layer was alternatively destroyed. It is attributed to the fact that the particle size of this armor layer is smaller than that of the others. However, it regained its original shape and particle arrangement after a few minutes. Therefore, despite the instability of the secondary armor layer, due to the decrease in the strength of the horseshoe vortex, because of increasing the depth of the scour hole and decreasing the intensity of transferring the secondary armor layer materials towards downstream, the equilibrium depth is ultimately obtained. The armor layer, despite its overall particle uniformity ($\sigma_g > 1$), comprises a mix of finer and coarser grains. Initially, turbulent eddies selectively wash away the finer particles, leaving the coarser fraction in place. As flow velocity increases over time, these eddies begin to erode the finer particles from the underlying bed material, transporting them downstream as suspended load. Exceeding a critical flow velocity generates eddies powerful enough to destabilize the armor layer. These particles are then scoured and transported downstream, contributing to the development of the scour hole. In general, according to the overall shape of the scoured area, three groups of scour patterns were observed (Table 4). Figure 7 shows the schematic configuration of the scoured holes for each group, as specified in Table 4. To compare the shape of the scour and to investigate the effect of the armor layer particle size and thickness on the shape and extent of the scoured area, equilibrium longitudinal scoured hole profiles were obtained by applying the image processing technique. An important point in these figures is that the spread of the scour hole downstream of the pier is limited, such that the angle of the scour hole upstream face with the piers does not exceed 60°. However, downstream of the pier, a longer scoured area is generated, resulting in a relatively flattened scoured bed; therefore, the secondary armor layer is limited to a small area L_s around the pier (Fig. 7c).

Table 4. General classification of the experiments under unsteady-state flow conditions.

Group No.	Test No.	Description
1	M_3, M_{12}, M_{18}	• The armor layer remains undamaged in the downstream and back of the pier. • Scour occurs due to the movement of the bed particles through the armor layer materials. • The scouring mechanism is alike the operation of a rip-rap layer.
2	M_2, M_6, M_{11}, M_{15}, M_{17}	• At the beginning of the experiment, the armor layer downstream and back of the pier is destroyed, but an accumulated secondary armor layer formed downstream of the piers. • The armor layer is destroyed and washed away to a short distance downstream. • Around the scoured area, the armor layer particles remain intact.
3	M_1, M_4, M_5, M_7, M_8, M_9, M_{10}, M_{13}, M_{14}, M_{16}	• The armor layer is destroyed and completely washed away downstream and the back of the pier. • The thickness of the secondary armor layer is equal to the median diameter of the armor particles. • The progress of the scouring downstream of the pier is quicker, resulting in a flattened scour hole downstream face.

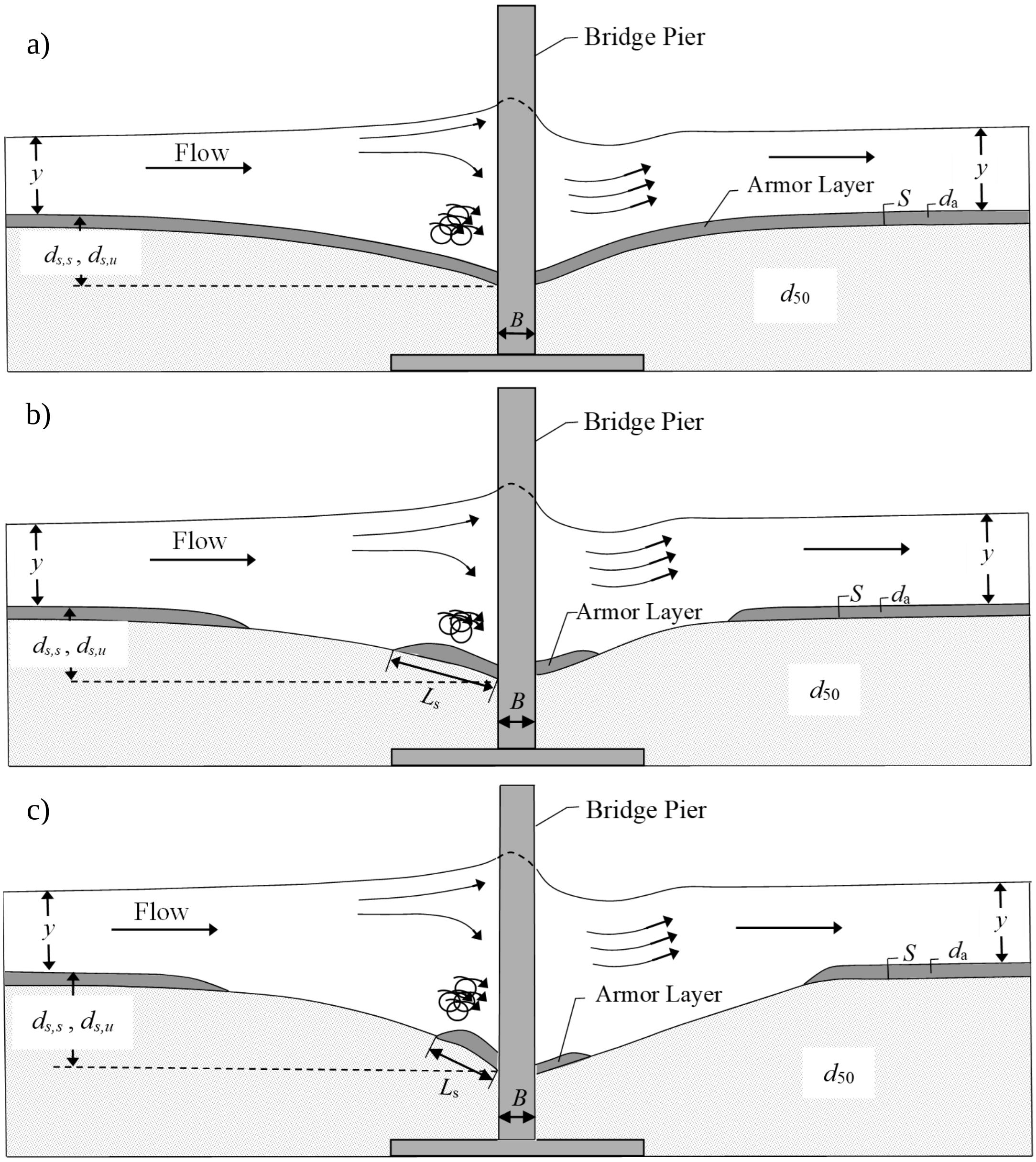

Fig. 7. Schematics of the scour hole at the bridge piers, concerning the observed classifications (a) Group 1, (b) Group 2, and (c) Group 3.

4.2 Unsteady Flow Case

According to Fig. 8, the type of triangular hydrograph with different base times affects the maximum scour depth at the bridge pier, such that as the base time of the hydrographs increases, the maximum scour depth increases. For example, for model M_7, hydrographs H_1, H_2, H_3, H_6, H_7, and H_8 are employed. With a 300% increase in the base time of the hydrographs, the maximum scour depth increases by about 11.3, 12.9, and 11.5% for H_1 to H_3, respectively, for model M_{10}, with a 300% increase in the hydrograph base time, the maximum scour depth increases by about 10.9, 15.8, and 3.8%; for model M_{13}, by about 9.7, 8.3, and 11.3%; for model M_{14}, by about 12, 13.7, and 12.2%; for model M_{16}, by about 7.4, 1.9, and 5.6%; and for model M_{17}, by about 1, 7.5, and 7.3%. According to Table 3, in model M_{17}, for hydrographs H_2, H_5, and H_7, the maximum scour depths were 0.037, 0.039, and 0.040 m, respectively. The base times of these hydrographs were 30, 60, and 120 min, respectively. With increases of 200% and 400% (relative to the 30-minute hydrograph base time) in the base time, the maximum scour depths increased by approximately 5.13% and 7.5%, respectively. For model M_1, with hydrographs H_2, H_5, and H_7, with 200% and 400% increases in the base time, the maximum scour depths increased by approximately 4% and 11.1%, respectively. Considering different hydrographs, the average maximum scour depths for models M_1 and M_{17} are 0.051 and 0.039 m, respectively. Models M_4, M_5, and M_6 have constant d_a/d_{50} ratios of 9.08 with pier diameters of 0.042, 0.033, and 0.022 m, respectively.

Based on the dimensional analysis, an important parameter affecting the maximum scour depth under unsteady-state flow conditions is d_a/d_{50}. Figure 9 shows the results for M_2, M_5, and M_{13} with hydrographs H_2, H_5, and H_7. According to Fig. 9a, by increasing d_a/d_{50} ($d_a/d_{50} \geq 9.08$), the dimensionless maximum scour depth decreases. For a better comparison, a set of hydrographs 2, 5, and 7 with base times of 30, 60, and 120 min, respectively, was included for the analysis. As the bed particle size increases, the maximum scour depth decreases. Furthermore, by increasing d_a/d_{50}, the maximum scour depth indicates increasing-decreasing trends for different hydrographs.

Due to the increase in the armor layer particle size, according to Table 3, for models M_1-M_2 and M_4-M_6, for all hydrographs, the rate of decrease is greater than that of the increasing trend. By increasing the average diameter of the armor layer particles or increasing the thickness of the armor layer, the gap between the dimensionless maximum scour depth trends for Hydrographs H_2 and H_7 increases, indicating the better protective effect of the armor layer with a coarser aggregate. Furthermore, the maximum scour depth increases as the average diameter of the bed material decreases, a trend consistent with the findings of Fathi et al. (2024, 2025a). Figure 9b shows the effect of the Froude number F, on the maximum scour depth under unsteady-state flow conditions for a constant pier diameter of 0.042 m. As illustrated, by increasing F or the flow velocity, the maximum scour depth increases. Under clear-water conditions, an increase in F intensifies vortices around the bridge piers, leading to a greater maximum scour depth. The relationship between pier diameter and scour depth is quantified in Table 3. For models M_4-M_6 (with a constant relative armor size, d_a/d_{50} = 9.08), a reduction in pier diameter (B) leads to a systematic decrease in both the absolute and relative scour depth. Specifically, as the pier diameter was reduced from 0.042 m to 0.033 m (-21.4%) and 0.022 m (-47.6%), the average maximum scour depth ($d_{s,u}$) decreased from 0.051 m to 0.043 m (-15.7%) and 0.023 m (-54.9%), respectively.

When expressed in the standard dimensionless form, the relative scour depth ($d_{s,u}/B$) for these cases was 1.21, 1.30, and 1.05. This trend of decreasing absolute scour depth with decreasing pier size was consistent across all other model configurations. Furthermore, Fig. 9c illustrates the influence of the hydrograph duration, expressed as dimensionless parameter TV_e/B, on the normalized maximum scour depth ($d_{s,u}/B$) for different values of F. The results demonstrate that an increase in the hydrograph base time leads to a significant increase in the dimensionless scour depth. While the shape of the triangular hydrographs had a minimal effect, their base time was a critical factor, consistent with the former findings (Maherani et al., 2010). For instance, for F = 0.185 and B = 0.042 m, a 200% and 400% increase in TV_e/B resulted in an increase of the normalized scour depth ($d_{s,u}/B$) by approximately 9.3% and 15.8%, respectively.

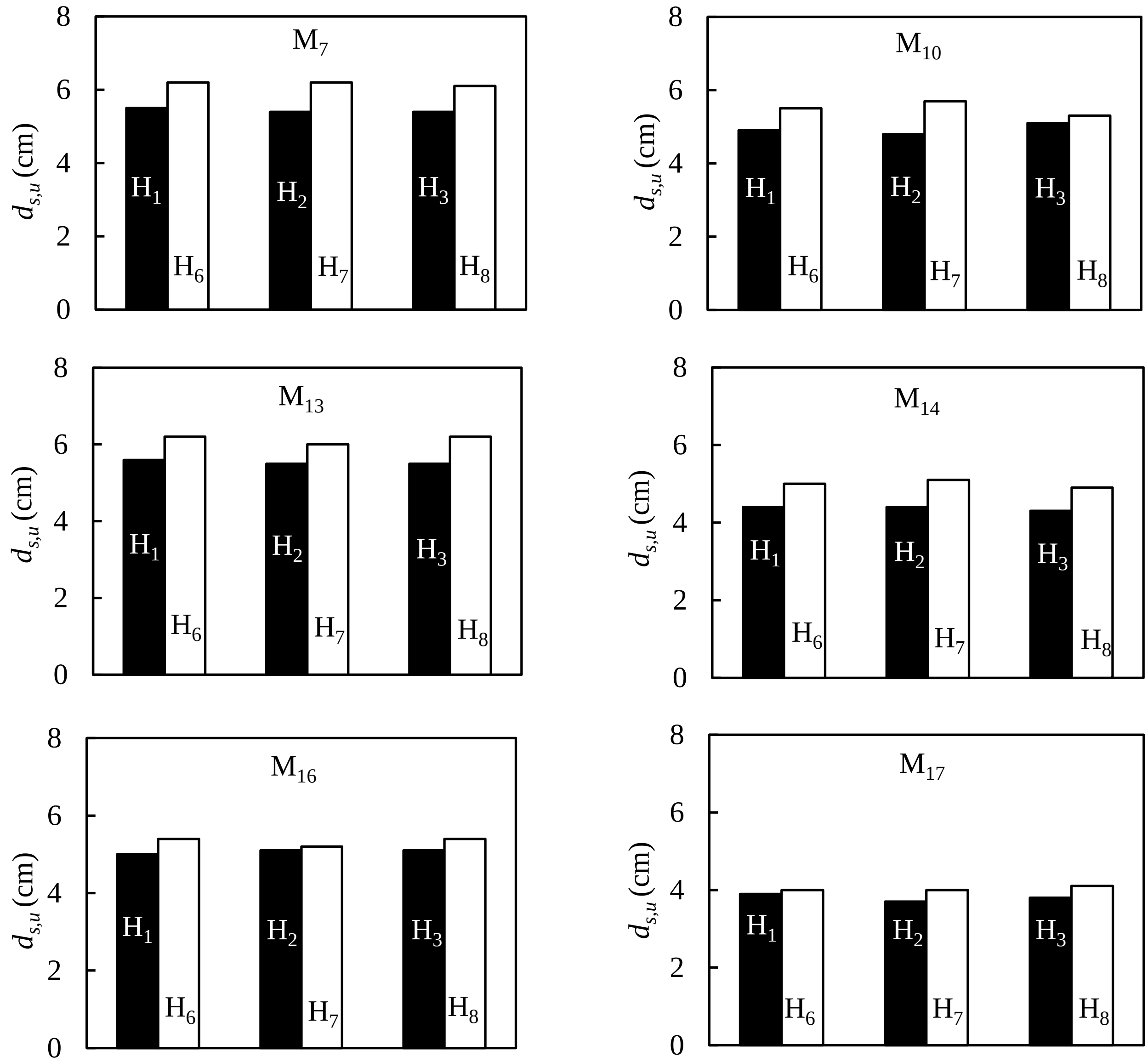

Fig. 8. The effect of hydrograph base time on maximum scour depth under unsteady flow conditions.

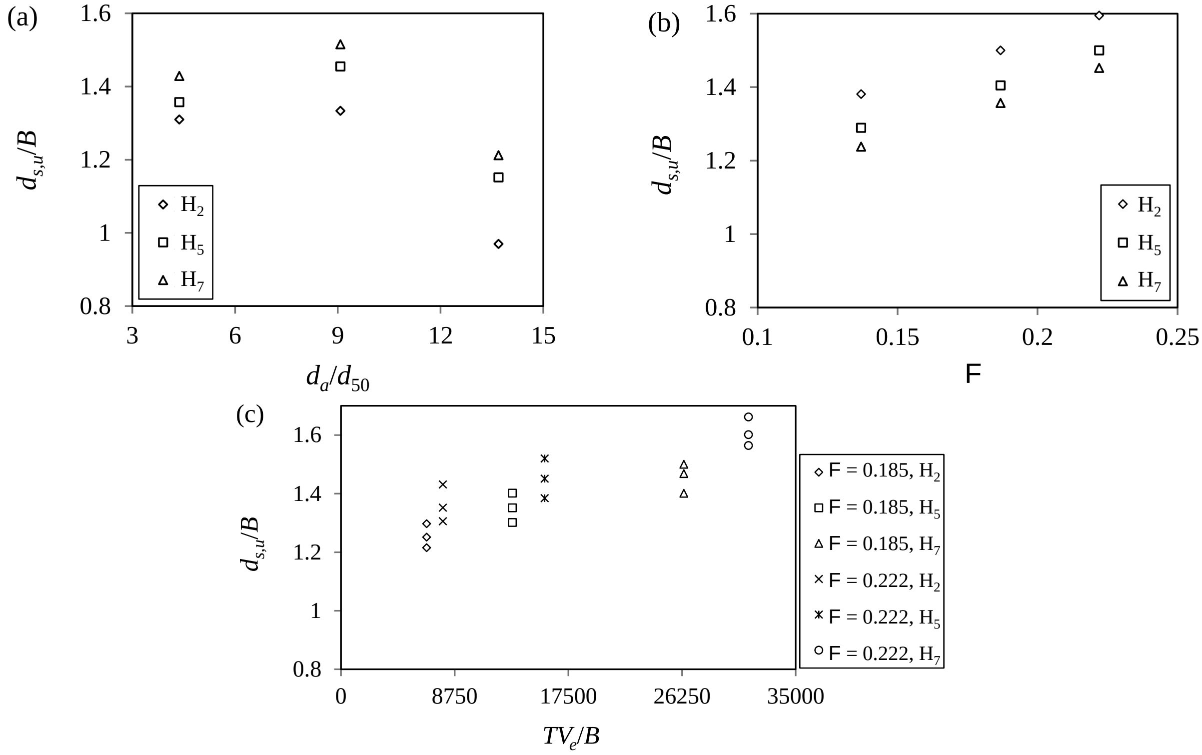

Fig. 9. The dimensionless maximum scour depth under unsteady-state flow conditions versus (a) d_a/d_{50}, (b) F, and (c) TV_e/B.

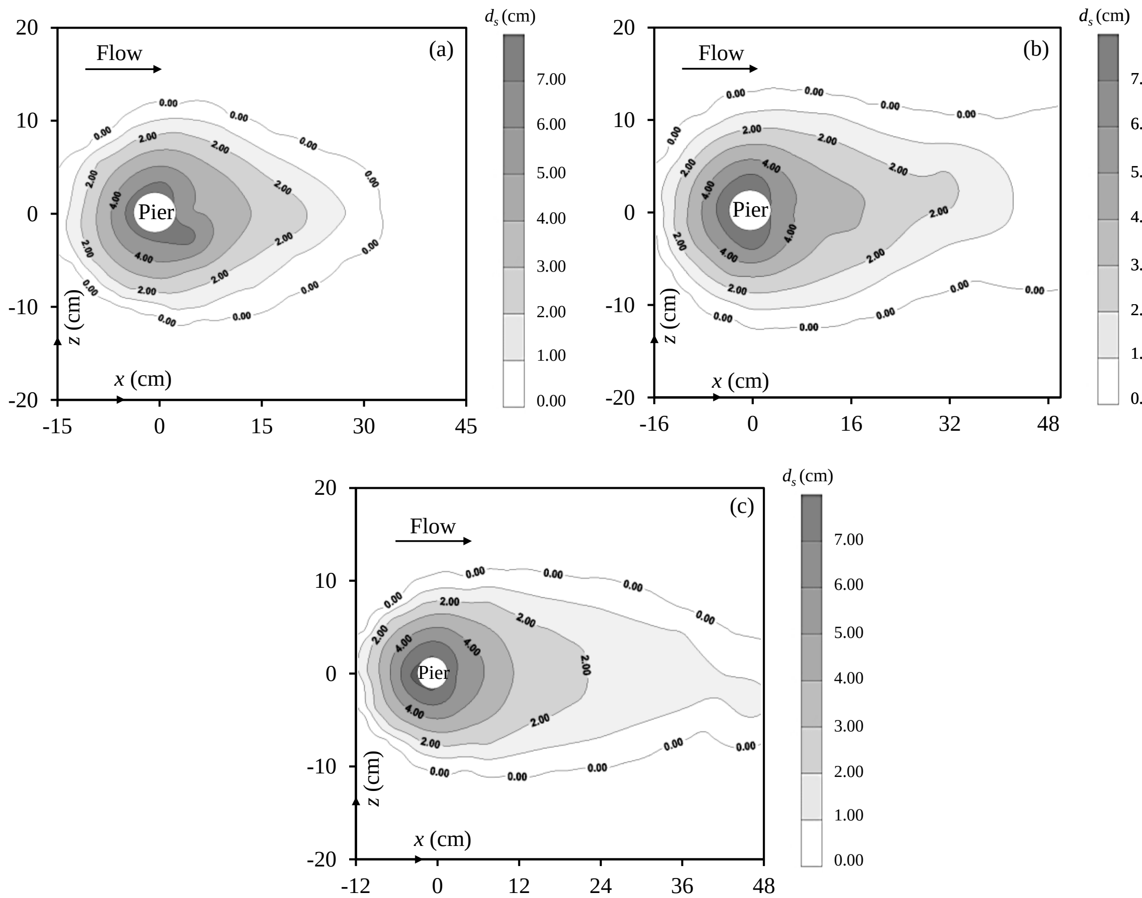

Fig. 10. Contour maps of the scour hole at the bridge piers for d_a/d_{50} = 9.08, considering hydrographs (a) H_1, (b) H_4, and (c) H_6.

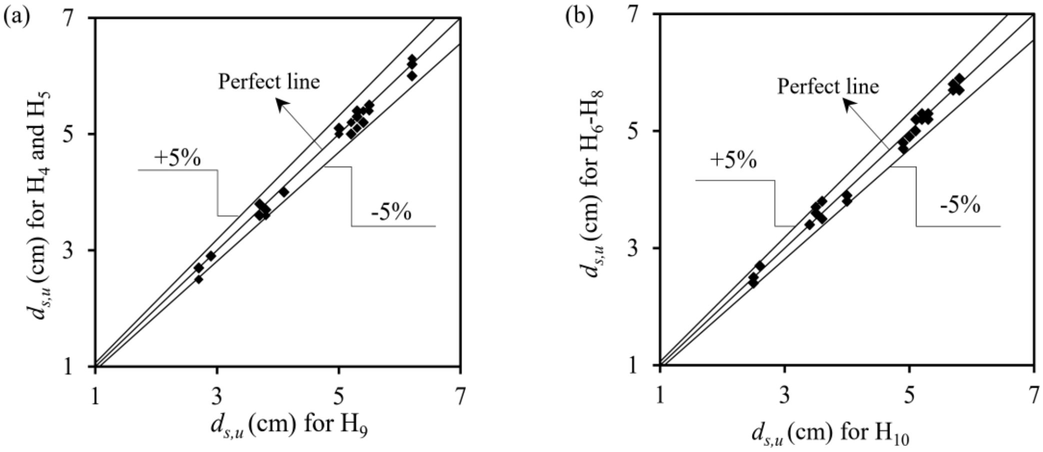

Fig. 11. Comparison of the results with respect to $d_{s,u}$ obtained from combined hydrographs against integrated hydrographs (a) H_9 against H_4 and H_5, and (b) H_{10} against H_6-H_8.

To examine the effect of hydrograph repetition on the maximum scour depth, the results of hydrographs H_9 and H_{10}, including 2 and 5 repetitions, respectively, are compared. The results indicated that the shape of the hydrograph has less effect on the maximum scour depth. However, the base time of the hydrograph has a significant effect on the scouring configuration. By increasing the hydrograph base time, the maximum scour depth increases, reaching a maximum value at the equilibrium time. The average maximum scour depths obtained for hydrographs H_9 and H_{10} were compared to the maximum scour depth in experiments without repetition with the same base time, e.g., 60 and 120 min, respectively.

Figure 11a compares the maximum scour depth for hydrograph H_9 (with two repeated 30-minute base time hydrographs) and those of the integrated hydrographs H_4 and H_5 with 60 60-minute base time. Figure 11b compares the maximum scour depth of hydrograph H_{10} (with five repeated 30-minute base time hydrographs) and that of the integrated hydrographs H_6 to H_8 with a 120-minute base time. As illustrated in Fig. 11, with an acceptable discrepancy (±5% scattering), the results of the combined and the corresponding integrated hydrographs are identical. Maherani et al. (2010) and Borghei et al. (2012) have also concluded that combination of the hydrographs has the least effect on scouring pattern.

As the number of repeating hydrographs increases, the maximum scour depth increases; however, repeating the same hydrograph with a constant base time and a momentary decrease in flow discharge, the shear stresses in the scoured hole decrease and then increase transitorily. The successive decrease and increase of the shear stress on the bed cause deviations in the scour hole depth, resulting in the successive erosion and filling of the bed materials as well as the armor layer particles. This process continues until the last iteration of the hydrographs. Finally, the maximum scour depth of the repeating hydrographs is relatively equal to that of the unit hydrograph with the same base time, with ±5% discrepancy.

By applying the dominant dimensionless parameters of Eq. (4), employing 80% data of the normalized maximum scouring depth at bridge piers in the presence of an armor layer under unsteady flow conditions, and using the SPSS mathematical software, Eqs. (9a) and (9b) were obtained, such that they precisely estimate $d_{s,u}/B$ for the remaining 20% verification data. The division into experimental and calibration groups followed the standard hold-out method (Karkheiran et al., 2021, and Fathi et al., 2025b). Figure 12 shows the observed and calculated maximum dimensionless scour depth under unsteady state flow conditions, with a scatter of ±10% compared to the 20% verification data.

$$\frac{d_{s,u}}{B} = \left(\frac{TV_e}{B}\right)^{0.09}\left[1 - 0.65\left(\frac{d_a}{d_{50}}\right)^{6.5F^3} F^{0.32}\right], \quad 0 < \frac{d_a}{d_{50}} \le 9.08 \tag{9a}$$

$$\frac{d_{s,u}}{B}1.21 = \left(\frac{TV_e}{B}\right)^{0.09}\left(\frac{d_a}{d_{50}}\right)^{-14.8F^3} F^{0.32}, \quad 9.08 \le \frac{d_a}{d_{50}} \tag{9b}$$

subject to the limitations of the present study, e.g., $4.19 \le d_a/d_{50} \le 13.69$, $0.137 \le F \le 0.307$, $4843 \le TV_e/B \le 59891$, and $\sigma_g \le 1.35$.

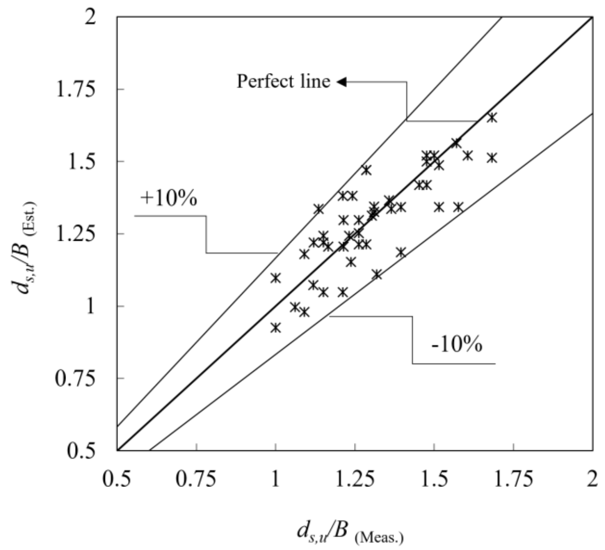

Fig. 12. Estimated versus measured dimensionless maximum scour depth at bridge piers under unsteady-state flow conditions.

As stated previously, after training, the models were evaluated on an independent test set. Their predictive performance was determined using three standard metrics: coefficient of determination (R^2), mean absolute error (*MAE*), and root mean square error (*RMSE*). These metrics are defined in Eqs. (10), (11), and (12), respectively.

$$R^2 = \frac{\left(\sum_{i=1}^{N}(t_i-\bar{t})(y_i\bar{y})\right)^2}{\sum_{i=1}^{N}(t_i-\bar{t})^2\sum_{i=1}^{N}(y_i-\bar{y})^2} \tag{10}$$

$$MAE = \frac{1}{N}\sum_{I=1}^{N}|y_i - t_i| \quad (11)$$

$$RMSE = \sqrt{\frac{1}{N}\sum_{I=1}^{N}(y_i - t_i)^2} \quad (12)$$

where N is the number of targets (observations), t_i is a target value, y_i is a predicted value, $\bar{t}$is the observed mean value, and $\bar{y}$is the predicted mean value. The coefficients R^2, *MAE*, and *RMSE* for Eq. (9a) are 0.934, 0.0335 and 0.0452, respectively, and for Eq. (9b) are and 0.965, 0.0343, and 0.0311, respectively. While both models perform very well, Eq. (9b) is unequivocally a better choice. It provides a tighter fit to the data (higher R^2), has a lower average error (lower *MAE*), and, most importantly, is more robust with fewer big problematic errors (significantly lower *RMSE* and a smaller *RMSE-MAE* gap). We conducted the initial data analysis using SPSS software. To ensure the robustness of our findings, we performed a sensitivity analysis implemented in MATLAB using a Genetic Algorithm (GA) as detailed by Karkheiran et al. (2021) and Fathi et al. (2025b). We assessed the accuracy of our models using two standard metrics: *RMSE* and R^2. We also tested the importance of each parameter by removing it from the model one at a time and recording the change in these metrics. The results are presented in Table 5. As shown in Table 5, F and TV_e/B are the most influential factors (R^2 = 0.853 and 0.871). The V_e, T, and the diameters of the armor layer and the bed material show less effects.

Figure 13 compares the present maximum scour depth with those of the other researchers. Karimaei and Zarrati (2019a) used a circular bridge pier with a diameter of 0.07 m, an average diameter of bed particles of 0.00067 m, and a pier Froude number of 1.06 under unsteady flow conditions. They investigated different hydrograph times between 0.42 and 90 hours. Karimaei and Zarrati (2019b) used a rectangular bridge pier with a width of 0.05 and a length of 0.25 m, with the pier Froude number of 1.53. The base time of the hydrographs in their study varied between 1 and 237 minutes. Melville and Chiew (1999) applied circular bridge piers with various diameters ranging from 0.016 to 0.2 m. The average flow velocity varied between 0.165 and 1.140 m s^{-1}. Considering different hydraulic/geometric parameters and different hydrograph base times compared to these of the present study, Eq. (9a) is not precisely capable of predicting the maximum scour depth based on the former research data.

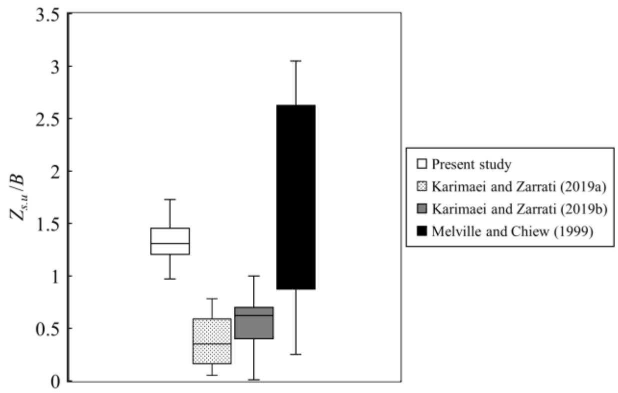

Fig. 13. Comparison of the maximum dimensionless scour depth calculated under unsteady flow conditions in the present study with those of the other researchers.

4.3 Steady Flow Case

By increasing F, the maximum scour depth increases, which is in part due to the increase in flow discharge and flow velocity. Due to the increase in grain size and armor layer thickness, which is in line with unsteady-state flow conditions, by increasing d_a/d_{50}, the maximum scour depth decreases. Two main issues involved in the expansion of the scouring area and destruction of the armor layer downstream of the pier are (i) the bed materials are significantly smaller than those of the armor layer, washing out at a higher rate. The collision of the washed-out particles from the hole imposes stresses on the armor layer particles, intensifying the scouring and increasing the probability of particle movement. (ii) Flow downstream of the pier changes the bed roughness through evacuation from the scouring hole, leading to an increase in the stresses applied to the armor layer boundary particles, expanding the scouring further downstream. Scouring under steady-state flow conditions can be considered as a special case of scouring under unsteady-state flow conditions.

Table 5. Sensitivity analysis for the normalized scour depth at the bridge pier under unsteady-state flow conditions.

Eq.	Dependent variable	Independent variables	Error indices		
			R^2	*MAE*	*RMSE*
9a	$d_{s,u}/B$	$F, \frac{d_a}{d_{50}}, \frac{TV_e}{B}$	0.934	0.0335	0.0452
		$F, \frac{d_a}{d_{50}}$	0.426	0.0622	0.0761
		$F, \frac{TV_e}{B}$	0.853	0.0473	0.0491
		$\frac{d_a}{d_{50}}, \frac{TV_e}{B}$	0.472	0.0649	0.0792
9b	$d_{s,u}/B$	$F, \frac{d_a}{d_{50}}, \frac{TV_e}{B}$	0.965	0.0311	0.0343
		$F, \frac{d_a}{d_{50}}$	0.456	0.0599	0.0723
		$F, \frac{TV_e}{B}$	0.871	0.0365	0.0456
		$\frac{d_a}{d_{50}}, \frac{TV_e}{B}$	0.493	0.0614	0.0694

In the present study, the ratio of the average diameter of the armor layer particles to the reference length d_a/R_L is 0.01 to 0.031 (R_L = $(B^2y)^{1/3}$). Consistent with Pandey et al. (2019), who considered d_a/R_L = 0.04-0.17, by increasing d_a/R_L, the maximum dimensionless scour depth $d_{s,s}/R_L$, decreases. It is concluded that by increasing the bridge pier diameter and the average diameter of the armor layer particles, likewise the steady-state flow condition, the maximum scour depth under the unsteady-state flow condition decreases.

Figure 14 shows the dimensionless maximum scour depth around the bridge pier versus t/t_e. Throughout each test, the bed profile is measured at regular intervals until the equilibrium state is achieved. For measurements at specific times, the procedure involved halting the flow and applying the image processing technique outlined in the Equilibrium Time, Image Processing, and Bed Topography section to determine the maximum scour depth. After each data collection event, the sediment bed was carefully leveled and compacted. The experimental conditions were then reset to a flow depth of 0.07 m, and the target discharge was set before commencing the subsequent test run. Ultimately, the maximum scour depth recorded at the equilibrium state using this method showed only negligible errors compared to the continuous test runs without interruption, validating the approach and ensuring results repeatability and accuracy. Figure 14a-c shows the equilibrium time with respect to the maximum scour depth for piers with 0.042, 0.033, and 0.022 m in diameter, respectively. Accordingly, for times up to $t = 0.2t_e$, the maximum scour depth increases significantly. Considering a constant d_a/d_{50}, models M_1, M_2, and M_3 highlight the effect of the pier diameter (e.g., 0.042, 0.033, and 0.022 m, respectively), suggesting that the maximum scour depth increases by increasing the pier diameter. The scouring equilibrium time for smaller pier diameters is shorter than that for larger pier diameters. The equilibrium times for models M_1 to M_3 are 1260, 1140, and 900 min, respectively. Compared to a pier diameter of 0.042 m, the equilibrium time decreases by approximately 6.3% and 13.7% when the pier diameter decreases by 21.43% and 47.62%, respectively. This is partly due to the increase in the armor layer thickness, which reduces the strength of the horseshoe vortices. As stated previously, the greatest fragment of the maximum scour depth occurs at $t = 0.2t_e$; afterwards, the scouring becomes very slow up to $t = 0.6t_e$, after which the rate of scouring decreases significantly. Consistent with Pandey et al. (2021), who investigated the maximum scour depth around the breakwaters, by increasing the scouring time, the maximum scour depth increases, becoming almost constant, while reaching the equilibrium time. This is partly because, at the equilibrium state, vortex strength has stabilized and is insufficient to cause sudden or excessive displacement of the bed and armor layers. Figure 14d compares the present results for models M_1 to M_3 with those of Abdi-Chooplou and Vaghefi (2023), Eshaghian et al. (2020), Taheri and Ghomeshi (2019), and Aghli and Zomorodian (2013), considering pier diameters of 0.05, 0.04, 0.025, and 0.05 m, respectively.

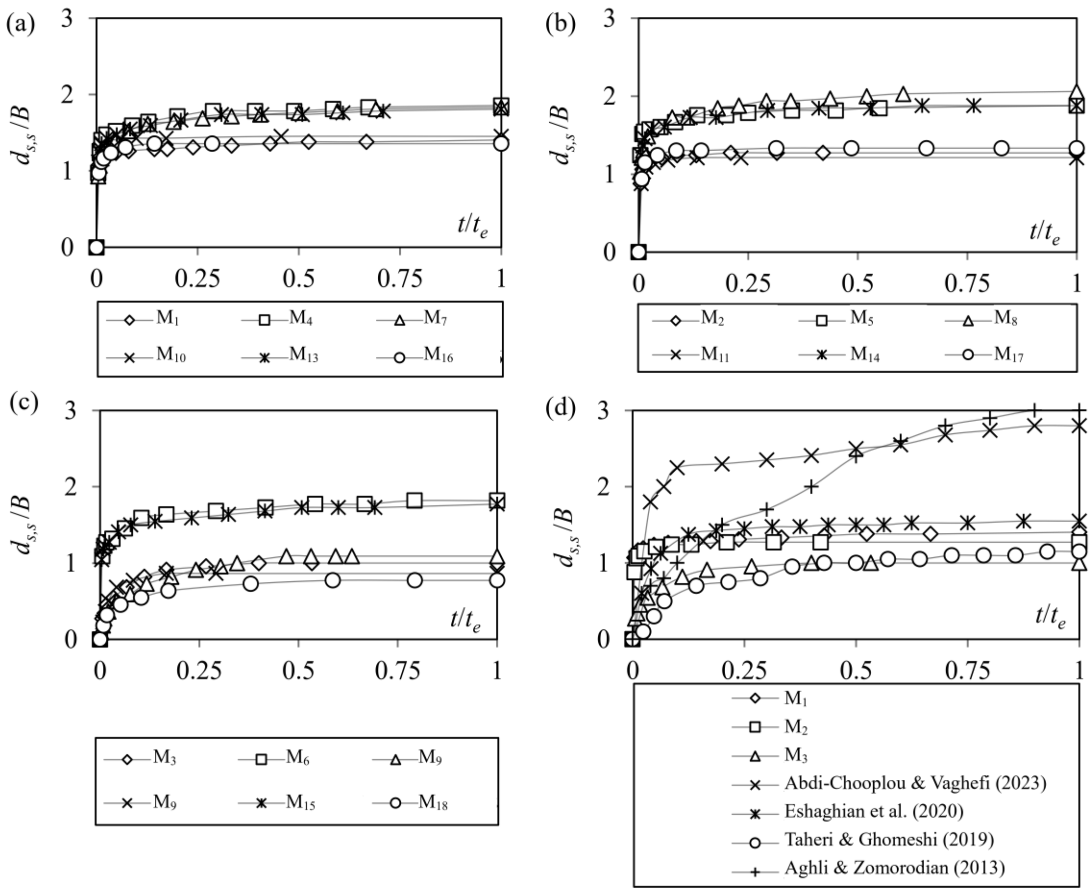

Fig. 14. The maximum scour depth at the bridge pier versus t/t_e under steady-state flow conditions (a) for B = 0.042 m, (b) for B = 0.033 m, (c) for B = 0.022 m, and (d) compared to the other studies.

In the experiments by Abdi-Chooplou and Vaghefi (2023), which featured a constant flow depth and submerged plates in a 180° bend with a velocity ratio (U/U_{ca}) of 0.98, the average maximum dimensionless scour depth was approximately 46% higher than in the present study. The larger bridge pier diameter in the experiments of Eshaghian et al. (2020) resulted in an average maximum dimensionless scour depth approximately 25% higher than that found in the present study, despite both investigations using a velocity ratio (U/U_{ca} = 0.50 to 0.95) and an armor layer. A comparison with the work of Taheri and Ghomeshi (2019) shows a greater maximum dimensionless scour depth in their study (Fig. 14d). This difference occurred despite a velocity ratio (U/U_{ca} = 0.91) and is likely due to their use of a larger, elliptical pier (0.225 m x 0.025 m) compared to our smaller, circular pier (B = 0.022 m). Aghli and Zomorodian (2013) experimentally investigated scour around a larger bridge pier (B = 0.05 m) at a velocity ratio of U/U_{ca} = 0.91. Their measured maximum dimensionless scour depth was greater than this of the present study, a result attributed to the larger pier width.

Using the dimensionless parameters from Eq. (5), we derived Eq. (13) to estimate the time-dependent maximum scour depth under steady-state flow conditions. Consistent with the derivation of Eq. (9), Eq. (13) was calibrated, using 80% of the dataset and validated by the remaining 20% of the data. Performance of Eq. (13) is shown in Fig. 15, in which the predicted versus observed values for the validation data demonstrate a scatter of ±7%. This high level of accuracy indicates that Eq. (13) provides a robust predictive model for maximum scour depth in armored streambeds under steady-state flow conditions.

$$\frac{d_{s,s}}{B} = exp\left[1.22\left(\frac{t}{t_e}\right)^{0.05}\right]\left[1 - 0.65\left(\frac{d_a}{d_{50}}\right)^{6.5F^3} F^{0.32}\right], \quad 0 < \frac{d_a}{d_{50}} \le 9.08 \qquad (13a)$$

$$\frac{d_{s,s}}{B} = 1.21exp\left[1.22\left(\frac{t}{t_e}\right)^{0.05}\right]\left(\frac{d_a}{d_{50}}\right)^{-14.8F^3} F^{0.32}, \quad 9.08 \le \frac{d_a}{d_{50}} \qquad (13b)$$

subject to the limitations of the present study, including 4.19 ≤ d_a/d_{50} ≤ 13.69, 0.137 ≤ F ≤ 0.307, 0 ≤ t/t_e ≤ 1, and σ_g ≤ 1.35.

The coefficients R^2, *RMSE*, and *MAE* for Eq. (13a) are 0.922, 0.0398 and 0.0334, respectively, and for Eq. (13b) are 0.901, 0.0742 and 0.0581, respectively. While both models perform very well, Eq. (13a) is unequivocally a better choice. We also used sensitivity analysis for the steady-state flow conditions. As shown in Table 6, F and t/t_e are the most influential factors (R^2 = 0.757 and 0.744). The d_a/d_{50} and B have less effects. Figure 16 depicts a comparison of the maximum scour depth in a steady flow condition of the present study with those of the other researchers. Valela et al. (2018) investigated a new design for bridge piers, using a bridge pier with a width of 0.09 m, two average bed grain sizes of 0.7 and 0.001 m (with d_a/d_{50} = 78.6 and 55, respectively), three flow depths of 0.10, 0.15, and 0.20 m, and four average flow velocities of 0.25, 0.30, 0.34, and 0.38 m s^{-1}, t/t_e = 1, and U/U_{ca} = 1.15. In their research, $d_{s,s}/B$ varies between 0.4 and 1.4, and Eq. (13b), with a 50% discrepancy, applies to calculate the maximum scour depth. Farooq et al. (2023) conducted experiments with an average bed particle size of 0.00096 m, a bridge pier width of 0.06 m, an average flow velocity of 0.37 m s^{-1}, a pier Froude number of 0.482, t/t_e = 1.0, U/U_{ca} = 0.93, and d_a/d_{50} = 1.0. Here, Eq. (13a) applies with a discrepancy of 3% for the maximum scoured depth. Abdi-Chooplou et al. (2023) used a 0.05 m bridge pier and an average diameter of bed particles of 0.0015 m in the presence of vane plates at different distances from the bridge pier, for different values of t/t_e, U/U_{ca} = 0.98, $d_{s,s}/B$ = 0 to 2.8, and a Froude number of 0.55. Employing vanes with different distances and angles to the bridge pier resulted in the indirect flow path; thereby applying Eq. (13a) to their data yields a 32.5% discrepancy.

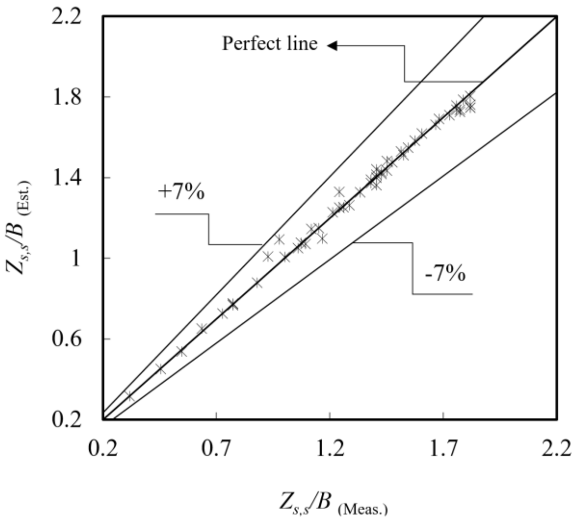

Fig. 15. The estimated against the measured dimensionless maximum scour depth at the bridge pier in the presence of an armor layer under steady-state flow conditions.

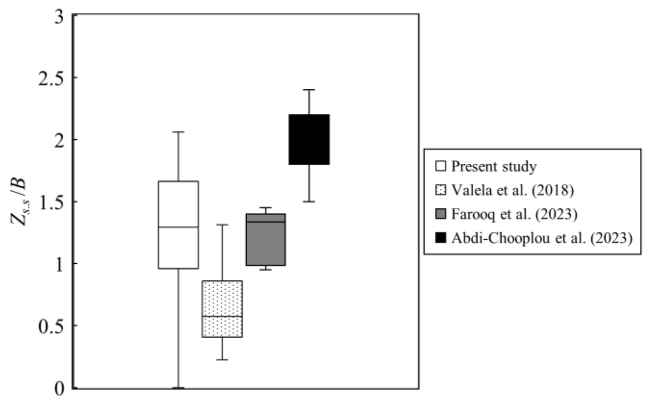

Fig. 16. Comparison of the maximum dimensionless scour depth calculated under the steady flow conditions in the present study with some studies by another researcher.

Figure 17a-c shows the longitudinal profiles of scour holes at bridge piers of 0.042, 0.033, and 0.022 m, respectively, under steady-state flow conditions, indicating that by increasing the pier diameter, the scour hole length increases. This is in part because, by decreasing the pier diameter, the strength of the vortices around the pier decreases. By increasing d_a/d_{50}, the area of the scour hole decreases. The armor layer reduces the dimensions of the scour hole, thereby at downstream of the bridge pier, a sedimentary hill is not generated. The armor layer covers the scour hole, reducing the amount of shear stress acting on the bed materials. The armor layer over the finer substrate prevents further scouring, while a sediment ridge forms downstream of the pier. However, as F and B increase, the amplified vortex strength reduces the height of this sediment ridge.

Table 6 Sensitivity analysis for the normalized scour depth at the bridge pier under steady-state flow conditions.

Equation	Dependent variable	Independent variables	Error		
			R^2	*MAE*	*RMSE*
13a	$d_{s,s}/B$	$F, \frac{d_a}{d_{50}}, \frac{t}{t_e}$	0.922	0.0334	0.0398
		$F, \frac{d_a}{d_{50}}$	0.613	0.0661	0.0702
		$F, \frac{t}{t_e}$	0.757	0.0522	0.0543
		$\frac{d_a}{d_{50}}, \frac{t}{t_e}$	0.287	0.0874	0.0973
13b	$d_{s,s}/B$	$F, \frac{d_a}{d_{50}}, \frac{t}{t_e}$	0.901	0.0581	0.0742
		$F, \frac{d_a}{d_{50}}$	0.586	0.0765	0.0923
		$F, \frac{t}{t_e}$	0.744	0.0628	0.0812
		$\frac{d_a}{d_{50}}, \frac{t}{t_e}$	0.221	0.0896	0.0987

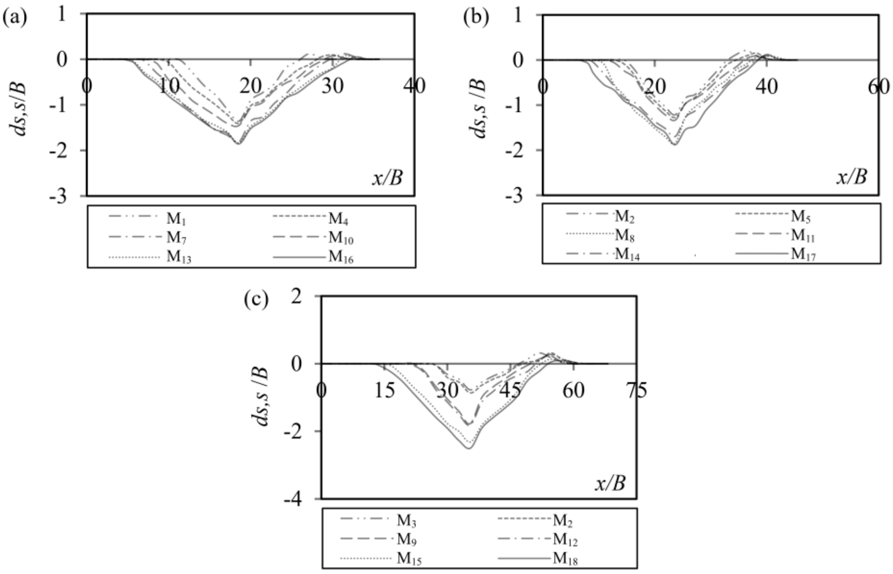

Fig. 17. Longitudinal scour profiles at the bridge piers for B = (a) 0.042 m, (b) 0.033 m, and (c) 0.022 m, under steady-state flow conditions.

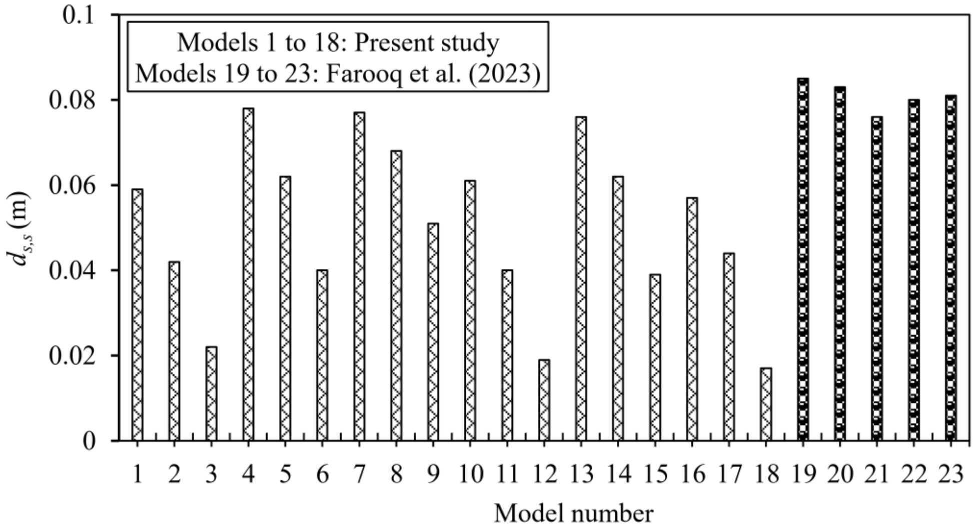

Fig. 18. The maximum scour depth in the present study compared to that of Farooq et al. (2023) under steady-state flow conditions.

Figure 18 compares the present results with those of Farooq et al. (2023), who experimentally studied scour at bridge piers with 0.09, 0.12, 0.15, 0.18, and 0.2 m in diameter. Due to the presence of an armor layer over the bed materials and the smaller diameter of the bridge piers, the present results are smaller than those of Farooq et al. (2023). They also investigated the effect of hook collars on local scouring at lenticular bridge piers. Compared to the bridge pier diameter of 0.042 m considered in the present study, by increasing the bridge pier diameter by 23.8%, 65%, 72%, 76.7%, and 79%, the maximum scour depth was increased by approximately 20%, 18.1%, 10.5%, 15%, and 16%, respectively. In this figure, models 1 to 18 refer to the present test models, and models 19 to 23 refer to the tests by Farooq et al. (2023).

Investigating the volume of scouring around the bridge piers is also one of the common problems of hydraulic engineers that has recently received attention. Figure 19 compares the scour volume under steady and unsteady flow conditions for a cylindrical bridge pier with an armor layer from the present study against results from other researchers using different pier shapes. The volume of the scoured hole under steady flow conditions for models M_1, M_4, and M_7 (bridge pier diameter of 0.042 m) is 0.004, 0.0048, and 0.0067 m^3, respectively. Increasing the shear stress on the bed material and the armor layer materials increases in scoured hole volume, by decreasing d_a/d_{50}. For the unsteady flow conditions with model M_4 and hydrographs H_1 to H_4, and H_6, respectively, the scour volume is 0.0039, 0.0038, 0.0039, 0.0046, and 0.0063 m^3, respectively. The scoured hole volume increases with the increase in the hydrograph base time. With a 200 and 300 percent increase in the base time of the hydrographs (H_4 and H_6) compared to that of H_1, the scour volume increases by about 15.2 and 38.1%, respectively. Due to the fixed time of the hydrograph, for hydrographs H_1 to H_3, the scoured hole volume is almost constant. The present results of scoured hole volume under the steady flow conditions are approximately identical to those of Sirianni et al. (2022), with a discrepancy of 1.4%. However, due to the application of a thin armor layer, the present results of scoured hole volume are significantly smaller than those of Farooq et al. (2023) and Abdi-Chooplou et al. (2023). Finally, the results of the scoured hole volume under steady flow conditions are greater than those under unsteady flow conditions.

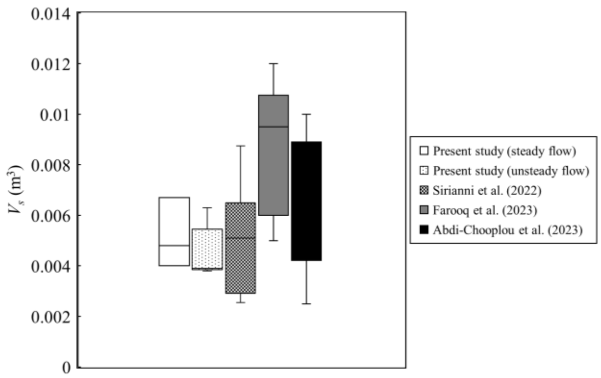

Fig. 19. Comparison of the volume of scour in the present study with some other studies by another researcher under steady and unsteady flow conditions.

5 CONCLUSIONS

In the present study, the effects of armoring on local scouring at bridge piers under steady- and unsteady-state flow conditions were investigated based on model experimentation. Given the significant differences in scouring under steady- and unsteady-state flow conditions, with the same peak flow discharge, designing a bridge pier based on scouring under steady-state flow conditions is not economical; therefore, the effects of flow unsteadiness should be considered by design engineers. Accordingly, the effects of the shape, base time, and repetition of the hydrographs on the equilibrium depth and shape of the scoured area in the presence of an armor layer were evaluated. The results indicated that the maximum scour depths due to the combined and integrated hydrographs were mostly identical. Under unsteady-state flow conditions, scouring at a bridge pier in an erodible bed covered with a thin layer of armor particles is independent of the shape of the hydrograph. By increasing the base time of the hydrograph, the dimensions of the scour hole increase significantly, and the angle of the scoured face downstream of the pier with respect to the horizontal plane decreases, resulting in expansion of the scoured zone upstream of the piers and a tendency to create a flat surface behind the piers. By applying the dominant dimensionless parameters, a double-criteria relationship with an acceptable precision was derived for estimating the maximum scour depth under unsteady-state flow conditions, considering triangular hydrographs.

Due to the continuous supply of armor materials at the upstream face of the hole, through the initial stages of the experiments, a relatively thick secondary armor layer was formed downstream of the pier, which was initially unstable, and the materials were continuously transferred downstream. By increasing the scour depth and decreasing the horseshoe vortex strength, the secondary armor layer was stabilized, resulting in an equilibrium scour depth. The minimum thickness of the stabilized secondary armor layer was equal to the diameter of the armor layer particles. Considering the overall shape of the scoured area, three types of scour patterns were observed, which were detailed in the present study. Examination of the scour patterns indicated that scour hole expansion, downstream of the pier, is constrained and the slope of its upstream face does not exceed 60°. Conversely, upstream of the piers, the bed is subjected to intense scouring that severely disrupts the armor layer. This erosion propagates the scoured area downstream, flattening the bed and leaving the armor layer intact only within a confined zone around the piers. The greatest changes in the maximum scour depth are established at $t \le 0.2t_e$. For $t \ge 0.6t_e$, the rate of scouring decreases greatly. Considering t/t_e as an effective dimensionless parameter for scouring under steady-state flow conditions, a double-criteria relationship was also derived for estimating the maximum scour depth under steady-state flow conditions in the presence of an armor layer.

This study has several limitations. The use of simplified triangular hydrographs and the assumption of a constant flow depth may not capture the complexity of natural flow conditions. Furthermore, the selected hydrograph base times of 30, 60, and 120 min are arbitrary, thereby future works should investigate a broader range of base time durations. The present study also has other limitations, such as its lab-scale nature, the use of a simplified hydrograph, and a lack of turbulence measurements (by LDV, PIV or ADV). Addressing these issues in future studies would be highly beneficial.

Acknowledgement: This research was conducted at the Utah Water Research Laboratory; the authors express their gratitude for the support provided to complete this research.

NOTATION

The following symbols are used in this paper:

A_s = surface area of the pond (m^2)

B = pier diameter (m)
d_a = median armor layer particle size (m)
d_{50} = median bed particle size (m)
F = Froude number (-)
g = Gravitational acceleration (m s^{-2})
H_i = hydrograph No. i (-)
h = the color depth (-)
I = inflow (m^3 s^{-1})
i = color intensity (-)
L_S = length of the secondary armor layer behind the pier (m)
M_i = model No. i (-)
N = number of targets (observations) (-)
n = number of hydrograph repetitions (-)
O = outflow (m^3 s^{-1})
R = Reynolds number (-)
R_L = reference length (m)
S = thickness of the armor layer (m)
S_V = storage volume of the reservoir (m^3)
T = base time of the hydrograph (s)
t = time (s)
t_e = equilibrium scour time (s)
t_i = target value (-)
$\bar{t}_m$ = observed mean value (-)
U = average flow velocity (m s^{-1})
U_{ca} = average critical flow velocity of the armor layer (m s^{-1})
$u*$ = critical shear velocity (m s^{-1})
$u*_{ca}$ = critical shear velocity of the armor layer (m s^{-1})
V_s = volume of scour around the bridge piers (m^3)
V_e = equivalent flow velocity (m s^{-1})
W = Weber number (-)
x = longitudinal direction (m)
y = flow depth (m)
y_i = predicted value (-)
$\bar{y}_m$ = predicted mean values (-)
$d_{s,s}$ = maximum scour depth under steady-state flow conditions (m)
$d_{s,u}$ = maximum scour depth under unsteady-state flow conditions (m)
μ = dynamic viscosity (kg m^{-1} s^{-1})
ρ_w = water density (kg m^{-3})
ρ_s = bed material density (kg m^{-3})
σ_g = uniformity coefficient of the bed materials (-)

REFERENCES

Abdi-Chooplou, C., and Vaghefi, M. 2023. Numerical study of upstream submerged vanes affecting bed in a sharp bend with a bridge pier via SSIIM software. Inno. Infra. Sol., 8(10): 1–18. https://doi.org/10.1007/s41062-023-01249-9

Abdi-Chooplou, C., Kahrizi, E., Fathi, A., Ghodsian, M. and Latifi, M., 2024. "Baffle-enhanced scour mitigation in rectangular and trapezoidal piano key weirs: An experimental and machine learning Investigation". Water, 16(15), p.2133. https://doi.org/10.3390/w16152133

Abdi-Chooplou, C., Vaghefi, M., and Akbari, M. 2023. "Effect of repositioned submerged vanes on local scour variations around a pier in a bend: experimental investigation." Int. J. Environ. Sci. Tech., 20(4): 1–14. https://doi.org/10.1007/s13762-023-05031-3

Ahmadi, R., Afzalimehr, H., Abed, H.J. and Okhravi, S., 2025. "Hydrodynamic effects of porous baskets on scour patterns at elliptical and hexagonal piers". Journal of Hydrology and Hydromechanics, 73(3), pp.230-247. https://doi.org/10.2478/johh-2025-0018

Aghli, M., and Zomorodian, S. 2013. "Effect of cable and collar on scouring depth around cylindrical bridge pier in meandering river." Irri. Sci. Eng., 36: 31–40. https://doi.org/20.1001.1.25885952.1392.36.3.4.9

Babakhah, L. and Khoshfetrat, A., 2024. "Investigating local scour downstream of Piano key weir with Riprap". Innovative Infrastructure Solutions, 9(11), pp.1-15. https://doi.org/10.1007/s41062-024-01759-0

Baranwal, A. and Das, B.S., 2024. "Live-bed scour depth modelling around the bridge pier using ANN-PSO, ANFIS, MARS, and M5Tree". Water Resources Management, 38(12), pp.4555-4587. https://doi.org/10.1007/s11269-024-03879-9

Bento, A.M., Gomes, A., Viseu, T., Couto, L. and Pêgo, J.P., 2020. "Risk-based methodology for scour analysis at bridge foundations." Engineering structures, 223, p.111115. https://doi.org/10.1016/j.engstruct.2020.111115

Bento, A. M., J. P. Pêgo, T. Viseu, and L. Couto., 2018. "Evolution of local pier scour under unsteady flow conditions" Proc. of the 5thIAHR Europe Congress — New Challenges in Hydraulic Research and Engineering. https://doi.org/10.3850/978-981-11-2731-1_384-cd

Borghei, S. M., Kabiri-Samani, A. R., and Banihashem, S. A. 2012. "Influence of unsteady flow hydrograph shape on local scouring around bridge pier." Proc. Inst. Civil Eng.-Water Manage., 165(9): 473–480. https://doi.org/10.1680/wama.11.00020

Chang, W. Y., Lai, J. S., and Yen, C. L. 2004. "Evolution of scour depth at circular bridge piers." J. Hydraul. Eng., 130(9): 905–913. https://doi.org/10.1061/(ASCE)0733-9429(2004)130:9(905)

Chaudhry, M.H., 2008. Open-channel flow (Vol. 523). New York: Springer. https://doi.org/10.1007/978-3-030-96447-4

Chiew, Y. M. 1992. "Scour protection at bridge piers." J. Hydraul. Eng., 118(9): 1260–1269. https://doi.org/10.1061/(ASCE)0733-9429(1992)118:9(1260)

Chow, V. T. 1959. Open channel hydraulics. Tokyo: McGraw-Hill Kogakusha.

Dah-Mardeh, A., Azizyan, G., Bejestan, M.S., Parsaie, A. and Rajaei, S.H., 2023. "Experimental study of variation sediments and effective hydraulic parameters on scour downstream of stepped spillway". Water Resources Management, 37(13), pp.4969-4984. https://doi.org/10.1007/s11269-023-03587-w

Dehghan, D., Vaghefi, M., and Ghodsian, M. 2023. "Effects of increasing the width of collar on reduction of scouring surrounding the rectangular piers in a 180-degree bend." Appl. Water Sci., 13(3): 1–13. https://doi.org/10.1007/s13201-023-01884-8

De Laine, R.J., 1964. "Calibration of weirs using the rate of pondage drawdown". Journal of hydrology, 2(2), pp.130-140. https://doi.org/10.1016/0022 -1694(64)90024-1

Delf Lovimi, M., Masjedi, A., Heidarnejad, M., Bordbar, A., and Kamanbedast, A. A. 2020. "Control of scour around the piles with using cable and collar at the river." Iran. J. Watershed Manag. Sci. Eng., 14(49): 40–49. https://doi.org/20.1001.1.20089554.1399.14.49.11.0

Dey, S., and Barbhuiya, A. K. 2004. "Clear-water scour at abutments in thinly armored beds." J. Hydraul. Eng., 130(7): 622–634. https://doi.org/10.1061/(ASCE)0733-9429(2004)130:7(622)

Dey, S., and Raikar, R. V. 2007. “Clear-water scour at piers in sand beds with an armor layer of gravels.” J. Hydraul. Eng., 133(6): 703–711. https://doi.org/10.1061/(ASCE)0733-9429(2007)133:6(703)

Einstein, H.A., 1950. “The bed-load function for sediment transportation in open channel flows (No. 1026)”. US Department of Agriculture.

Eshaghian, M., Gohari, S., and Okhravi, S. S. 2020. “Single bridge pier scouring in uniform and non-uniform sediment beds under steady and unsteady flow.” J. Hydraul., 14(4), 19–33. https://doi.org/10.30482/JHYD.2019.198223.1405

Farooq, R., Azimi, A. H., Tariq, M. A., and Ahmed, A. 2023. “Effects of hooked-collar on the local scour around a lenticular bridge pier.” Int. J. Sed. Res., 38(1): 1–11. https://doi.org/10.1016/j.ijsrc.2022.07.002

Farooq, R., Ghumman, A.R., Ahmed, A., Latif, A. and Masood, A., 2021. “Performance evaluation of scour protection around a bridge pier through experimental approach.” Tehnički vjesnik, 28(6), pp.1975-1982. https://doi.org/10.17559/TV-20200213211932

Fathi, A., Abdi Chooplou, C., and Ghodsian, M. 2024. “Local scour downstream of type-A trapezoidal stepped PKW in sand and gravel sediments”. ISH Journal of Hydraulic Engineering, pp. 1–13. https://doi.org/10.1080/09715010.2024.2353612

Fathi, A., Khoshfetrat, A. and Alavi, S.H., 2025a. “Downstream Local Scour of PKW with Different Shapes and Numbers of Flow Splitters”. Journal of Hydraulic Engineering, 151(4), p.04025015. https://doi.org/10.1061/JHEND8.HYENG-14143

Fathi, A., Khoshfetrat, A., Talebipour, F. and Saadat, M., 2025b. “Influence of rigid vegetation on flow energy dissipation downstream of type B trapezoidal piano key weirs.” Innovative Infrastructure Solutions, 10(8), pp.1-15. https://doi.org/10.1007/s41062-025-02172-x

Fiorentini, M. and Orlandini, S., 2013. “Robust numerical solution of the reservoir routing equation”. Advances in Water Resources, 59, pp.123-132. https://doi.org/10.1016/j.advwatres.2013.05.013

Gaudio, R., Tafarojnoruz, A., and Calomino, F. 2012. “Combined flow-altering countermeasures against bridge pier scour.” J. Hydraul. Res., 50(1): 35–43. https://doi.org/10.1080/00221686.2011.649548

Ghasemzadeh, F., Kouchakzadeh, S. and Belaud, G., 2020. “Unsteady stage-discharge relationships for sharp-crested weirs”. Journal of Irrigation and Drainage Engineering, 146(6), p.04020009. https://doi.org/10.1061/(ASCE)IR.1943-4774.0001468

Guo, J., 2020. “Empirical model for shields diagram and its applications”. Journal of Hydraulic Engineering, 146(6), p.04020038. https://doi.org/10.1061/(ASCE)HY.1943-7900.0001739

Guo, J., 2012. “Pier scour in clear water for sediment mixtures”. Journal of hydraulic research, 50(1), pp.18-27. https://doi.org/10.1080/00221686.2011.644418

Gupta, L.K., Pandey, M., Raj, P.A. and Pu, J.H., 2023. “Scour reduction around bridge pier using the airfoil-shaped collar”. Hydrology, 10(4), p.77. https://doi.org/10.3390/hydrology10040077

Hager, W.H. and Sinniger, R., 1985. “Flood storage in reservoirs”. Journal of irrigation and drainage engineering, 111(1), pp.76-85. https://doi.org/10.1061/(ASCE)0733-9437(1985)111:1(76)

Hager, W. H., and Unger, J. 2010. “Bridge pier scour under flood waves.” J. Hydraul. Eng., 136(10): 842–847. https://doi.org/10.1061/(ASCE)HY.1943-7900.0000281

Hashemi, F.M., Khoshfetrat, A., Izadinia, E. and Delavari, E., 2025. “Investigating the Discharge Coefficient in Crump Weirs Under Increasing Flow Rate Conditions (Unsteady Flow)”. Iranian Journal of Science and Technology, Transactions of Civil Engineering, pp.1-16. https://doi.org/10.1007/s40996-025-01986-0

Hsiao, M., Lichter, S., and Quintero, L. G. 1988. “The critical Weber number for vortex and jet formation for drops impinging on a liquid pool.” Physics Fluids, 31(12): 3560–3562. https://doi.org/10.1063/1.866872

Kabiri-Samani, A. R., 2012a. “Armoring effect on local scouring around the bridge pier under steady flow (Part 1).” Journal of Hydraulics, 6(4): 59-75 (in persian). https://doi.org/10.30482/jhyd.2012.85409

Kabiri-Samani, A. R., 2012b. “Armoring effect on local scouring around the bridge pier under unsteady flow (Part 2).” Journal of Hydraulics, 7(2), pp.13-26 (in persian). https://doi.org/10.30482/JHYD.2013.15751

Kabiri-Samani, A. R., and Naderi, S. 2017. “Turbulent structure in the transition from super-to subcritical flow without a hydraulic jump.” J. Hydraul. Res., 55(1): 50–62. https://doi.org/10.1080/00221686.2016.1212939

Kandasamy, J. K., and Melville, B. W. 1998. “Maximum local scour depth at bridge piers and abutments.” J. Hydraul. Res., 36(2): 183–198. https://doi.org/10.1080/00221689809498632

Karimaei, T. M., and Zarrati, A. R. 2019a, “Local scour depth at a bridge pier protected by a collar in steady and unsteady flow.” Proc. Instit. Civil Eng.-Water Manage. 172(6): pp. 301–311. https://doi.org/10.1680/jwama.18.00061

Karimaei, T. M. and Zarrati, A. R. 2019b. “Estimation of time development of local scour around rectangular bridge pier in an unsteady flow condition.” J. Hydraulics, 14(4): 49–64. https://doi.org/10.30482/JHYD.2019.139858.1308

Karkheiran, S., Kabiri-Samani, A. R., Zekri, M. and Azamathulla, H. M., 2021. “Scour at bridge piers in uniform and armored beds under steady and unsteady flow conditions using ANN-APSO and ANN-GA algorithms.” ISH Journal of Hydraulic Engineering, 27(1): 220-228. https://doi.org/10.1080/09715010.2019.1617796

Kisi, O., Ardiçlioğlu, M., Hadi, A.M., Kuriqi, A. and Kulls, C., 2023. “Estimation of mean velocity upstream and downstream of a bridge model using metaheuristic regression methods”. Water Resources Management, 37(14), pp.5559-5580. https://doi.org/10.1007/s11269-023-03618-6

Kothyari, U. C., Garde, R. C. J., and Ranga Raju, K. G. 1992. “Temporal variation of scour around circular bridge piers.” J. Hydraul. Eng., 118(8): 1091–1106. https://doi.org/10.1061/(ASCE)0733-9429(1992)118:8(1091)

Link, O., Henríquez, S., and Ettmer, B. 2018. “Physical scale modelling of scour around bridge piers.” J. Hydraul. Res., 57(2): 227–237. https://doi.org/10.1080/00221686.2018.1475428

Lim, F. H., and Chiew, Y. M. 2001. “Parametric study of riprap failure around bridge piers.” J. Hydraul. Res., 39(1): 61–72. https://doi.org/10.1080/00221680109499803

Mahdavi, S.M., Izadinia, E. and Khoshfetrat, A., 2024. “Discharge Coefficient Calibrations of Normal and Oblique Circular-Crested Weirs Under Incremental Flow Conditions”. Iranian Journal of Science and Technology, Transactions of Civil Engineering, 48(4), pp.2679-2689. https://doi.org/ 10.1007/s40996-023-01277-6

Maherani, M., Kabiri-Samani, A., and Afzalimehr, H. 2010. "Armored layer bed effect on local scouring around bridge abutment." J. Hydraulics, 5(1): 1–19. https://doi.org/10.30482/JHYD.2010.85415

Melville, B. W., and Chiew, Y. M. 1999. "Time scale for local scour at bridge piers." J. Hydraul. Eng., 125(1): 59–65. https://doi.org/10.1061/(ASCE)0733-9429(1999)125:1(59)

Melville, B. W., and Sutherland, A. J. 1988. "Design method for local scour at bridge piers." J. Hydraul. Eng., 114(10): 1210–1226. https://doi.org/10.1061/(ASCE)0733-9429(1988)114:10(1210)

Misuriya, G. and Eldho, T.I., 2023. "Turbulent structures and local scour around a cylindrical pier under unsteady flows". Environmental Fluid Mechanics, 23(6), pp.1359-1380. https://doi.org/ 10.1007/s10652-023-09951-z

Moncada-M, A. T., Aguirre-Pe, J., Bolívar, J. C., and Flores, E. J. 2009. "Scour protection of circular bridge piers with collars and slots." J. Hydraul. Res., 47(1), 119–126. https://doi.org/10.3826/jhr.2009.3244

Muzzammil, M., and Siddiqui, N. A. 2009. "A reliability-based assessment of bridge pier scour in non-uniform sediments." J. Hydraul. Res., 47(3): 372–380. https://doi.org/10.1080/00221686.2009.9522008

Okhravi, S., Gohari, S., Alemi, M. and Maia, R., 2022. "Effects of bed-material gradation on clear water scour at single and group of piles". Journal of Hydrology and Hydromechanics, 70(1), pp.114-127. https://doi.org/10.2478/johh-2021-0036

Pandey, M., Chen, S.C., Sharma, P.K., Ojha, C.S.P. and Kumar, V., 2019. "Local scour of armor layer processes around the circular pier in non-uniform gravel bed". Water, 11(7), p.1421. https://doi.org/10.3390/w11071421

Pandey, M., Karbasi, M., Jamei, M., Malik, A. and Pu, J.H., 2023. "A comprehensive experimental and computational investigation on estimation of scour depth at bridge abutment: emerging ensemble intelligent systems". Water Resources Management, 37(9), pp.3745-3767. https://doi.org/10.1007/s11269-023-03525-w

Pandey, M., Valyrakis, M., Qi, M., Sharma, A. and Lodhi, A.S., 2021. "Experimental assessment and prediction of temporal scour depth around a spur dike". International Journal of Sediment Research, 36(1), pp.17-28. https://doi.org/10.1016/j.ijsrc.2020.03.015

Parker, G. 2008. "Transport of gravel and sediment mixtures". In Sedimentation Engineering: Processes, Measurements, Modelling and Practice, Edited by M. Garcia, 165–251.

Raikar, R. V., and Dey, S. 2009. "Maximum scour depth at piers in armor-beds." KSCE J. Civil Eng., 13: 137–142. https://doi.org/10.1007/s12205-009-0137-1

Ranjbar-Zahedani, M., Keshavarzi, A., Khabbaz, H., and Ball, J. E. 2021. "Optimizing flow diversion structure as an effective pier-scour countermeasure." J. Hydraul. Res., 59(6): 963–976. https://doi.org/10.1080/00221686.2020.1862321

Raudkivi, A. J., and Ettema, R. 1984. "Scour at cylindrical bridge piers in armored beds." J. Hydraul. Eng., 111(4): 713–731. https://doi.org/10.1061/(ASCE)0733-9429(1985)111:4(713)

Raudkivi, A. J., and Ettema, R. 1983. "Clear-water scour at cylindrical piers." J. Hydraul. Eng., 109(3): 338–350. https://doi.org/10.1061/(ASCE)0733-9429(1983)109:3(338)

Sammen, S.S., Amini, A., Othman Ahmed, K., Sadeghifar, T., Pushparaj, J. and Naganna, S.R., 2025. "Improving Bridge Safety: A Spider Monkey Optimization-based ANN Model for Scour Depth Prediction". Water Resources Management, pp.1-23. https://doi.org/10.1007/s11269-025-04224-4

Solati, S., Vaghefi, M., and Ahmadi, G. 2023. "Scour pattern around a pier in a 180° sharp bend: influence of pier shape under unsteady currents." Hydro. Sci. J., 68(12): 1711–1723. https://doi.org/10.1080/02626667.2023.2236089

Solati, S., Vaghefi, M., Ahmadi, G. and Behroozi, A.M., 2024. "Scouring and bed morphology dynamics in a sharp bend with collared pier under unsteady flow". Hydrological Sciences Journal, 69(15), pp.2227-2248. https://doi.org/10.1080/02626667.2024.2401086

Sui, J., Afzalimehr, H., Kabiri-Samani, A. R., and Maherani, M. 2010. "Clear-water scour around semi-elliptical abutments with armored beds." Int. J. Sediment Res., 25(3): 233–245. https://doi.org/10.1016/S1001-6279(10)60041-8

Taheri, Z., and Ghomeshi, M. 2019. "Experimental study of the effect of netted collar position on scour depth around of oblong-shappe bridge pier." Amirkabir J. Civil Eng., 51(2): 257–266. https://doi.org/10.22060/CEEJ.2017.13352.5388

Tipireddy, R.T. and Barkdoll, B.D., 2019. "Scour reduction by air injection at a cylindrical bridge pier: Experimental determination of optimal configuration". Journal of Hydraulic Engineering, 145(1), p.06018016. https://doi.org/10.1061/(ASCE)HY.1943-7900.0001555

Vaghefi, M., Asadollahi, M. and Behroozi, A., 2025. "Three-dimensional flow field analysis in a 180-degree bend with six- Pier groups positioned at various locations using SSIIM software". Innovative Infrastructure Solutions, 10(4), pp.1-24. https://doi.org/ 10.1007/s41062-025-01965-4

Valela, C., Nistor, I., Rennie, C.D., Lara, J.L. and Maza, M., 2021. "Hybrid modeling for design of a novel bridge pier collar for reducing scour. Journal of Hydraulic Engineering, 147(5), p.04021012. https://doi.org/10.1061/(ASCE)0733-9429(2000)126:1(43)

Valela, C., I. Nistor, and C. D. Rennie. 2018. "Reduction of bridge pier scour through the use of a novel collar design." In Proc., 6th Int. Disaster Mitigation Specialty Conf. 2018; Canadian Society for Civil Engineering, 235–244. Fredericton, Canada: Canadian Society for Civil Engineering. https://ruor.uottawa.ca/items/fcc4d286-3434-4138-837b-bd915022a46e

Valela, C., Whittaker, C.N., Rennie, C.D., Nistor, I. and Melville, B.W., 2022. "Novel riprap structure for improved bridge pier scour protection". Journal of Hydraulic Engineering, 148(3), p.04022002. https://doi.org/10.1061/(ASCE)HY.1943-7900.0001967

Van Rijn, L. C. 1984. "Sediment transport, part III: bed forms and alluvial roughness." J. Hydraul. Eng., 110(12): 1733–1754. https://doi.org/10.1061/(ASCE)0733-9429(1984)110:12(1733)

Veldhuizen, R., Broekema, Y. and Bruinsma, N., 2023. "Scour development in layered soils around offshore monopile foundations." In Proceedings of the 11th International Conference on Scour and Erosion. https://www.issmge.org/publications/publication/scour-development-in layered-soils-around-offshore-monopile-foundations

Wang, C., Yu, X., and Liang, F. 2017. "A review of bridge scour: mechanism, estimation, monitoring and countermeasures." Nat. Haz., 87: 1881–1906. https://doi.org/10.1007/s11069-017-2842-2

Wang, C., Yuan, Y., Liang, F., and Tao, J., 2022. "Experimental investigation of local scour around cylindrical pile foundations in a double-layered sediment under current flow." Ocean Engineering, 251, p.111084. https://doi.org/10.1016/j.oceaneng.2022.111084

Zefzouf, M., Chioukh, N., Castro, M., Miranda, F., Sousa, R.L., Carvalho, E., Rosa-Santos, P., Taveira-Pinto, F. and Fazeres-Ferradosa, T., 2025. "Laboratory study on scour development around a monopile in layered soils." Ocean Engineering, 342, p.122968. https://www.sciencedirect.com/science/article/pii/S0029801825026514

Zhou, K., Duan, J. G., and Bombardelli, F. A. 2020. "Experimental and theoretical study of local scour around three three pier group." J. Hydraul. Eng., 146(10), 04020069. https://doi.org/10.1061/(ASCE)HY.1943-7900.0001794

Received 3 October 2025
Accepted 12 January 2026